Annual Letter Report for April 1, 2009 to December 31, 2009

Project Title:	Nye County Ventilation Modeling and Support
Author and PI:	George Danko, Ph.D.
Co-Investigator:	Davood Bahrami, Ph.D.
Report Period:	April 1, 2009-December 31, 2009
Date of Report:	January 21, 2010

Table of Contents

Executive Summary

Three work elements are described for the reported period as Task 1 through Task 3 as follows:

Task 1- UZ PC activities assessment

We reviewed the Department of Energy (DOE) UZ PC plans and related documentation and provided the NWRPO with an assessment of the adequacy of the proposed monitoring activities. We developed recommendations for further in-drift PC activities necessary to monitor and characterize near-field conditions once waste packages are emplaced in the drift(s).

Task 2 –Modeling and assessment support for Nye County contentions

We continued numerical studies with MULTIFLUX (MF) 5.0 under the Oversight Project to document the underlying data and quantitatively substantiate any related contentions to the DOE License Application (LA) submitted by NWRPO. These tasks did not have new numerical code development components, and were restricted to the use of a given code. The results of the studies may be used to contribute to the contentions drafted by others.

There are a number of design parameters affecting the performance of the YM repository. One factor is the length of unheated sections. We further studied the waste emplacement layouts with various unheated drift sections as it was varied in the revisions of the model studies in the LA. It has been previously shown that the long unheated sections can improve the environmental condition of the heated section of the emplacement drifts. On the other hand, the reduction of the unheated sections has an opposite effect. The final design in the LA applies a rather short, 15 m long unheated section at the end of the emplacement drift, referred to as exhaust standoff. We have found that this 15-m distance is too short to avoid water condensation around the waste packages during the first 2000 years. The abstraction in the LA of not having condensation in the heated section in the first 2000 year of the drift is contradicted with the selected waste package layout.

In view of the new model simulation results for a representative emplacement drift, it appears that the abstractions in the LA do not hold against a real, coupled, comprehensive numerical study. In any future studies for Yucca Mountain, including design and performance confirmation, a new modeling approach must be adopted, applying fully-coupled thermal-hydrologic model elements for the in-rock and in-drift domains. Such a modeling method is demonstrated in Nye County's studies in 2009.

Task 3 – Corrosion-related studies

We studied the long-term post-closure thermal-hydrologic environment that affects corrosion. Quantitative prediction of humidity and liquid water in the selected emplacement drift during post-closure was specified with the new model and submitted to NWRPO and John Walton, another NWRPO contractor. These studies may be used to support Nye County contentions or evaluation of those submitted by other parties.

The results of these tasks are summarized in this annual letter report. Detailed technical description of part of the work and the results are also included in a journal paper, accepted for publication as follows:

1. Danko, G., Birkholzer J., Bahrami, D., Halecky, N. (accepted and edited for publication in 2009). *Temperature, Humidity and Air Flow in The Emplacement Drifts Using Convection and Dispersion Transport Models*, Journal of Nuclear Technology.

Additionally, a paper was published at the TOUGH 2009 symposium and presented in the Poster session as follows:

1. Danko, G., Birkholzer, J. T., Bahrami, D. (presented in 2009). *Development and Applications of a Turbulent Transport Network Model Coupled with TOUGH2*, TOUGH 2009 Symposium, September 14, 2009, Berkeley CA.

Introduction

Several different geometrical emplacement arrangements as well as assumptions and conditions have been considered by DOE in various model-elements of the LA. We have followed those with the corresponding model configurations and studied every one of them with the MF 5.0 model. Please refer to Table 1 for a summary of model arrangements.

Table 1. Summary of models used for Yucca Mountain project related to ventilation studies and Nye County contentions.

Modeling Arrangement		Model description
1	3-D Mountain-scale model Lawrence Livermore National Laboratory (LLNL)	Multi-scale thermal hydrologic model (MSTHM). No unheated section and no axial moisture transport is considered [1].
2	monolithic-scaled down model (LLNL)	3-D monolithic, three-drift, scaled-down model for validation of MSTHM calculations. Dispersion coefficient between 0.011 and 0.021 m^2/s for high dispersion case [1].
3	Panel-scale model Nye County, University of Nevada, Reno (UNR)	Used approximate modeling to simulate panel-scale model by removing an estimated percentage of WP heat in each emplacement drift for modeling panel edge effect. Predicted liquid water redistribution over one panel [2].
4	Pillar-scale model Sandia National Laboratory (SNL) and BSC	Various dispersion multipliers. recalculated the MSTHM, (2007). The dispersion used in the MSTHM report ranges between 0.028 and 0.042 m^2/s. No unheated section is included. [1]
5	Condensation model SNL and BSC	In-drift condensation model with one-dimensional dispersion. Drift wall is at saturated pressure. Dispersion values reported as high as 0.1 m^2/s [3,4].
6	Condensation model Lawrence Berkeley National Laboratory (LBNL)	Various dispersion coefficients (0.1 m^2/s for strong mixing and 0.004-0.008 m^2/s for moderate mixing), symmetrical unheated sections (80 m at both ends) [5].
7	Pillar-scale model LBNL and UNR	Effect of un-heated sections using 0.1 m^2/s dispersion coefficient [6].
8	Pillar-scale model Nye County and UNR	Effect of pre-closure ventilation period [7].
9	Pillar-scale model Nye County and UNR	Effect of barometric pressure pumping [8].
10	Pillar-scale model LBNL and UNR	Dispersive model with constant dispersion coefficient (0.1 m^2/s), symmetrical unheated sections (80 m at both ends) and line-load heat [9].
11	Pillar-scale model LBNL and UNR	Convective model with symmetrical unheated sections (80 m at both ends) and line-load heat [9].
12	Pillar-scale model LBNL and UNR	Dispersive model with back-calculated dispersion coefficient (old method), symmetrical unheated sections (80 m at both ends) and line-load heat [9].
13	Pillar-scale model Nye County and UNR	Convective model, symmetrical unheated sections (80 m at both ends), and variable heat load [10].
14	Pillar-scale model Nye County and UNR	Variable dispersion coefficient back-calculated using a new method (2009), line-load heat and symmetrical unheated sections (80 m at both ends) [11]
15	Pillar-scale model Nye County and UNR	Dispersive in-drift model with line-load heat, 0.1 m^2/s dispersion coefficient, symmetrical unheated sections (80 m at both ends) , with improved iterations[11].
16	Pillar-scale model Nye County and UNR	Dispersive in-drift model with variable heat load and, 0.1 m^2/s dispersion coefficient, and symmetrical unheated sections (80 m at both ends) [11].
17	Pillar-scale model Nye County and UNR	Dispersive in-drift model with variable heat load, 0.1 m^2/s dispersion coefficient, and asymmetrical unheated sections (65 m and 15 m at either end) [12].
18	Pillar-scale model Nye County and UNR	Convective in-drift model with variable heat load, asymmetrical unheated sections (65 m and 15 m at either end), and OBI iteration [12].
19	Pillar-scale model Nye County and UNR	Convective in-drift model with line-load heat, symmetrical unheated sections (80 m at both ends) with OBI iteration [13].
20	Pillar-scale model Nye County and UNR	Dispersive model with temperature-dependent air molecular dispersion coefficients with 1000 multiplication factor, variable heat load, no unheated sections, and OBI iteration [discontinued].
21	Pillar-scale model Nye County and UNR	Diffusive model with temperature-dependent air molecular dispersion coefficients with 1 multiplication factor, with variable heat load, no unheated sections and OBI iteration [discontinued].
22	Pillar-scale model Nye County and UNR	Dispersive model with temperature-dependent air molecular dispersion coefficients with 1000 multiplication factor, variable heat load, asymmetrical unheated sections (65 m and 15 m at either end), and OBI iteration [12].
23	Pillar-scale model Nye County and UNR	Diffusive model with temperature-dependent air molecular dispersion coefficients with 1 multiplication factor, variable heat load, asymmetrical unheated sections (65 m and 15 m at either end), and OBI iteration [12].

The LA documents use abstracted models of physical processes present at Yucca Mountain (YM) repository site. The basic model for the storage environment of the waste packages is established in the Mountain-Scale Thermal Hydrologic Model (MSTHM) Report [1]. The MSTHM assumes three-dimensional heat transport and moisture transport within the rockmass but no axial heat nor moisture transport inside the emplacement drift. Figure 1 illustrates the model assumptions regarding heat and moisture flow direction in the drift and the near-field rockmass. The MSTHM Report concludes that the effect of convective and/or diffusive heat and moisture transport inside the drift air space is not significant to be included in the Performance Assessment (PA) and other DOE models. The MSTHM Report's design layout of the emplacement drift applies no unheated section at the drift ends, and a symmetrical arrangement along the length of the emplacement drift. This assumption is different from the latest design variation in the LA which refers to asymmetrical unheated sections, that is, 60-m and 15-m empty sections at either ends of the emplacement drift. No significance has been attributed to these unheated sections since the in-drift transport processes are rendered insignificant in the PA studies. This case, referred to as "diffusive model" in this report (Model arrangement 23 in Table 1), is modeled with MF 5.0 to establish a basis for comparison with other arrangements within the same modeling environment,.

DOE's convection and condensation report by Webb [3, 4] applied a temperature boundary condition predicted by the MSTHM and an assumption of 100% relative humidity (RH) on the drift wall. Figure 2 illustrates the in-drift transport processes including their connection to the near-field rockmass in the convection and condensation studies [3, 4]. Inside the drift air space, a one-dimensional, dispersion coefficient-based transport model was used to study vapor condensation. Using an essentially uncoupled model from the thermal-hydrologic processes present in the near-field rockmass, the in-drift processes are poorly portrayed in the LA. The need for improvements was recognized, and follow-up studies were reported.

Buscheck included a new monolithic model study in the latest revision of the MSTHM report using Webb’s dispersion coefficient data, albeit with a value not as high as Webb suggested. This case is referred to as "dispersive model" in this report (Model arrangement 22 in Table 1).

Birkholzer et. al [5] studied in-drift axial transport with equivalent dispersion using Webb’s data [3, 4]. The LBNL monolithic model [5] used a symmetrical arrangement with 80-m unheated section and an enhanced in-drift dispersion coefficient of 0.1 m^2/s all in TOUGH2. Figure 3 illustrates the heat and moisture transport processes in the LBNL model [5].

The Nye County model provides the most realistic picture of the coupled in-drift and near-field transport processes in a selected emplacement drift. Figure 4 illustrates the heat, mass and airflow transport processes in the Nye County model [12]. This case is referred to as "convective model" in this report (Model arrangement 18 in Table 1).

The Nye County model results is presented in more detail as part of this annual report. In the next section the activities performed in 2009 are re-iterated and summarized under three assigned tasks, Task 1 through Task 3.

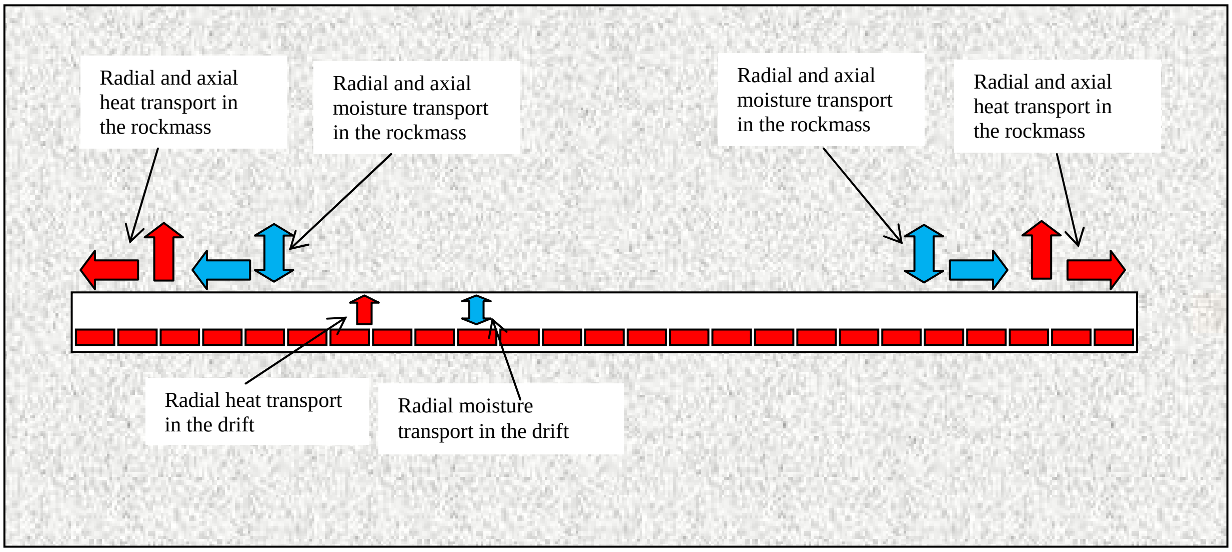

Figure 1. Overall model assumption in the MSTHM in the LA [1] with no unheated section.

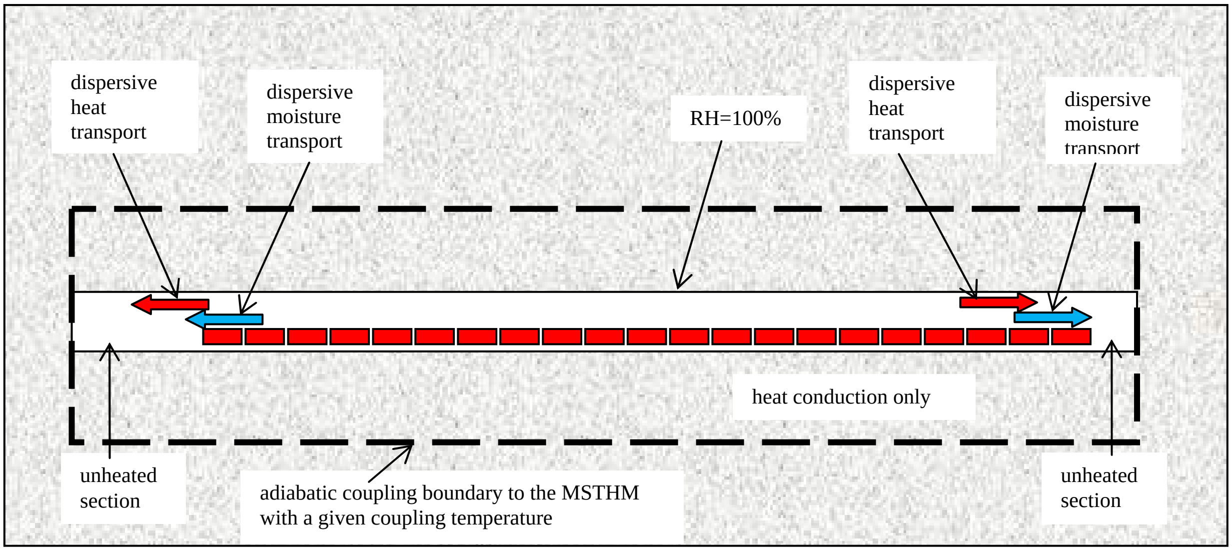

Figure 2. In-drift model process in the Natural Convection and Condensation Report [3].

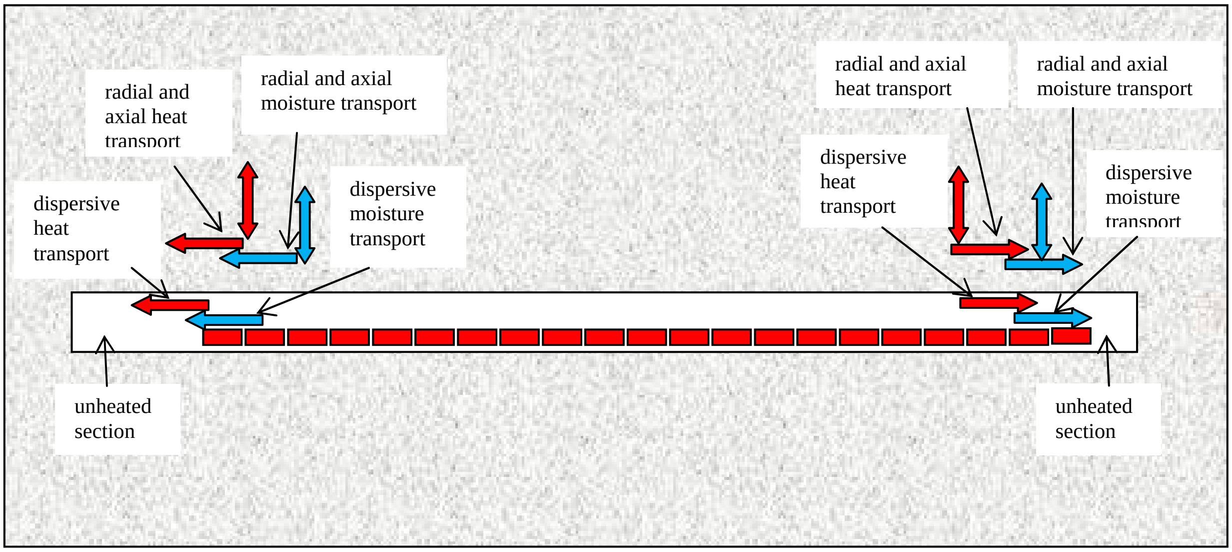

Figure 3. In-drift and in-rock transport processes in LBNL's monolithic TOUGH2 model [5].

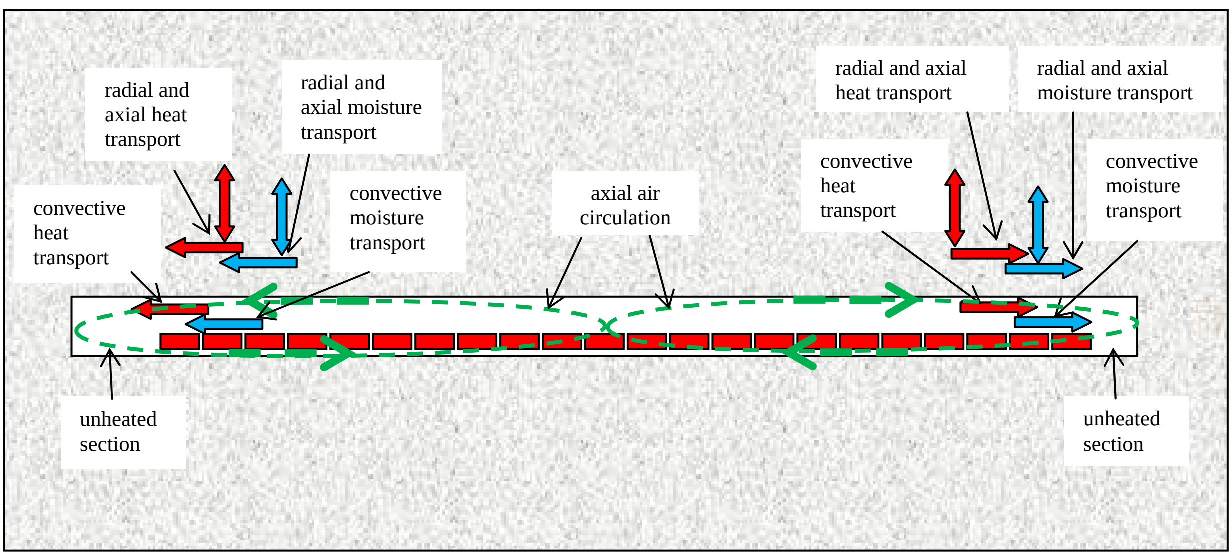

Figure 4. In-drift and in-rock transport processes in Nye County's thermo-hydrologic model with in-drift convection [12].

1. Task 1- UZ PC activities assessment

1.1. Review of the Performance Confirmation Plan

We have studied the performance confirmation plan focusing on the adequacy of the proposed monitoring activities. We recommend additional monitoring activities to understand in-drift seepage as it is affected by natural ventilation in the drift air space.

We studied the pillar-scale model of LA documents and updated our base dispersion coefficient input data using a temperature and time-dependent axial dispersion coefficient. Previously, constant dispersion coefficient of 0.1 m^2/s was used in our comparative studies (Model Arrangement 16 in Table 1) as the highest reported value in DOE documentations [3].

The newest results from the fully-iterated MF model indicate a much higher equivalent coefficient, reaching about 1 m^2/s. This new value is determined by matching the most realistic, axial convective model to an equivalent dispersion model. The new value of 1 m^2/s is about 40 times higher than that used by DOE in the LA models.

The scope of the program consists of tests, monitoring activities, and analyses to evaluate the adequacy of assumptions, data, and analyses that lead to the findings that permitted construction of the repository and subsequent emplacement of wastes (10 CFR 63.102(m)).

Performance confirmation monitoring is designed to focus on areas important to evaluating information supporting assessments of repository performance relative to the regulatory post-closure objectives or where uncertainties in the performance assessments result in high potential risk.

The approach used for selecting the set of activities (measured parameters and data acquisition methods) for evaluating the postclosure performance of the repository was based on three criteria and a decision analysis process, incorporating the definition of risk, applied to a set of parameters identified by subject matter experts.

- How important is the parameter to barrier capability and system performance?
- What is the level of confidence in the current knowledge about the parameter?
- How accurately can information be obtained by a particular test activity?

Performance confirmation began during the characterization of the Yucca Mountain site and will continue during repository construction and through operational emplacement of waste. Performance confirmation tests that will continue beyond site characterization, are as follows:

- Precipitation monitoring (precipitation quantities and composition measured at the Yucca Mountain site
- Seepage monitoring (seepage monitoring and analysis in alcoves on the repository intake side and in repository thermally accelerated drifts)
- Subsurface water and rock testing (chloride mass balance and isotope chemistry analysis of water samples collected at selected underground locations)
- Unsaturated zone testing (field-testing of transport and sorptive properties of unsaturated zone rock in an ambient seepage alcove or a drift with no waste packages emplaced)

- Saturated zone monitoring (measurements of water level, electrochemical potential, hydrogen potential, and background radionuclide concentrations in saturated zone wells at the repository site and in Nye County)
- Saturated zone alluvium testing (tracer testing of alluvium transport properties in the Alluvial Test Complex)
- Subsurface mapping (mapping of fractures, faults, stratigraphic contacts and lithophysal characteristics of rock in the underground openings)
- Seismicity monitoring (monitoring of regional seismic activity and observation of fault displacements following significant seismic events)
- Construction effect monitoring (measurement of construction deformation of underground openings/confirmation of related rock mechanical properties)
- Corrosion testing (laboratory samples testing of waste package, waste package pallet, and drip shield materials corrosion behavior in the range of expected repository environments)
- Waste form testing (laboratory testing of waste form dissolution and waste package coupled effects including use of scale mockups of waste package).
- New activities that will begin during construction or operations phases include:
- Saturated zone fault zone hydrology testing (hydraulic and tracer testing in fault zones).
- Drift inspection (periodic inspection of emplacement drifts and thermally accelerated drifts using remote inspection and measurement techniques).
- Thermally accelerated drift near-field monitoring (monitoring of rock mass and water properties in the near-field of a thermally accelerated emplacement drift).
- Dust buildup monitoring (monitoring and laboratory evaluations of quantity and composition of dust on engineered barrier surfaces and samples).
- Thermally accelerated drift environment monitoring (monitoring and laboratory evaluations of environmental conditions in a thermally accelerated drift including gas and water compositions, temperatures, film depositions, microbes, radiation and radiolysis effects using remote techniques).
- Thermally accelerated drift thermal-mechanical effects monitoring (monitoring of drift and invert degradation in a thermally accelerated drift).
- Seal testing (testing of effectiveness of borehole seals in the laboratory, shaft and ramp seals in the field, and backfill emplacement techniques).
- Waste package monitoring (monitoring of integrity of waste packages using visual inspection and/or internal pressure measurement employing remote monitoring techniques).
- Corrosion testing of thermally accelerated drift samples (laboratory testing of waste package, waste package pallet, and drip shield samples obtained from the thermally accelerated drift).

There are a number of problems with the monitoring activities planned in the PC document. We summarize the result of our findings and suggestions regarding these monitoring activities. The basic problem is that none of the monitoring activities, including the accelerated drift, can verify the post-closure in-drift storage environment conditions. Those conditions will still rely on model predictions. The PC plan, however, does not address the verification of the adequacy of model parameters and processes in the predictive models. In-drift natural convection and condensation processes are not planned to be monitored in the PC plan.

Four performance confirmation activities studied in light of our new thermal-hydrologic air flow studies:

- Seepage monitoring [14, Sec. 3.3.1.2];
- Unsaturated zone testing [14, Sec. 3.3.1.4];
- Thermally accelerated drift near-field monitoring [14,, Sec. 3.3.1.9]; and
- Thermally accelerated in-drift environment monitoring.

The problem is that conditions relative to in-drift induced thermal-hydrologic seepage will not be adequate for representing the conditions during the post-closure thermal time period of up to 10,000 years.

1.1.1 Seepage monitoring

Activities required for validating seepage are described in the safety analysis report: *"The purpose of this activity is to evaluate results from the seepage model and to evaluate unsaturated zone flow in the rock strata above the repository discussed in Section 2.3.3. Seepage monitoring results are used to evaluate: (1) the spatial and temporal distribution of seepage in the drifts and, if possible, to obtain samples of the seepage water for chemical analysis; and (2) the thermal loading effect on the spatial and temporal extent of seepage and on water chemistry (BSC 2004 [DIRS 172452], Section 3.3.1.2)"* (OCRWM, 2008 [LSN DEN001592183], p. 4-16)

Seepage monitoring is described in Sec. 3.3.1.2 p.p. 3-19 - 3-23 of PCP. *"This activity includes seepage monitoring, and lab analysis from bulk headed alcoves, on the intake side of the repository and in the thermally accelerated drifts."* [14, Sec. 3.3.1.2]

The principal activities proposed by the applicant to assess the adequacy of the assumptions, data, and analyses that support modeling of the features and processes that contribute to and provide the basis for the stated capability of the upper natural barrier (UNB) to prevent or substantially reduce the amount and rate of water seeping into the emplacement drifts are limited to the following: 1) monitoring of present-day precipitation and 2) monitoring of seepage at ambient (or near-ambient) temperatures and at representative repository temperatures in thermally accelerated drifts. [14, Table 3-1, p. 3-2, Table 3-2, p. 3-4, and p. 3-9; 15, p. 4-13].

Thermally-induced effects are further described: *"Seepage will be monitored at two types of locations: (1) in bulkheaded (i.e., unventilated) alcoves or boreholes at near-ambient temperature; and (2)an unventilated thermally accelerated drift to detect thermally driven seepage into a heated and unventilated drift which represent conditions most typical of the postclosure repository."* [14,Section 3.2; 15, p. 4-13]

A secondary activity involves subsurface water and rock testing (information potentially related to fast paths and percolation history for UZ flow model). [3,Table 3-1, p. 3-2, Table 3-2, p. 3-4, and p. 3-10; 15, SAR p. 4-13] UZ testing is planned, but it focuses on radionuclide transport processes relevant to the UZ transport model for evaluating the capability of the UZ feature of the LNB. [14, Table 3-2, p. 3-4, p. 3-26; 15, p. 4-19].

The performance confirmation activities are limited to precipitation and seepage monitoring, [15, Table 4-1; SAR p. 4-43 to 4-47] and do not address the adequacy of the basis for modeling the features and processes assessed in evaluating the capability of the UNB with regard to the in-drift induced thermal-hydrologic seepage process.

1.1.2 Unsaturated zone testing

Current project understanding is that seepage into the emplacement drift and flow by capillary diversion around the drift together equals the water flow rate to the lower natural barrier (LNB) [14, Sec. 3.3.1.4; 15, Sec 4.2.1.4]. In view of the Nye County model studies, this understanding is incorrect for the high temperature operating mode with drift sections at below-boiling temperature since percolation water flux will be redistributed into focused locations via condensation to the drift wall and under the drip shield.

1.1.3 Thermally accelerated drift near-field monitoring

This activity does not test the thermal-hydrologic seepage that enters the emplacement drift due to condensation. The coupled processes between the near-field rock and in-drift environment are not included, although the stated purpose of this activity is " *to evaluate coupled process results from the thermal-hydrologic-chemical-mechanical models. This activity monitors the near-field properties in the immediate vicinity of the thermally accelerated drift walls and serves as a surrogate for anticipated conditions during the thermal pulse and resulting permanent changes that may result after the thermal pulse in the fractured unsaturated rock above and below the repository subsides.* " [14, p. 2[a]].

The problem with the approach is that the in-drift induced thermal-hydrologic coupled processes will play within the same emplacement drift, and not in neighbor locations: *"Activities planned in a thermally accelerated drift will monitor in-drift conditions, expose engineered barrier material samples to potential corrosion mechanisms in representative in situ environments, monitor drift degradation, and test near-field coupled processes. The thermally accelerated drift conceptual design includes a thermally accelerated drift at the repository horizon and an observation and instrumentation drift at a lower elevation (Section 1.3.3.1). Completion of the instrumentation and baseline measurements in the thermally accelerated drift (Section 1.3.3.1) will be accomplished early in the waste emplacement period. The thermally accelerated drift thermal-mechanical monitoring performance confirmation activity described in Section 4.2.2 will also be conducted in a thermally accelerated drift (SNL 2008a, Section 3.3.1.2)."* [15, p. 4-15].

The performance confirmation document states that " *Changes in the near-field environment during the thermal pulse could change seepage patterns and compositions as well as drift stability. Section 3.3.2.4 complements this activity*." [14, p. 3-41]. and " *Based on results from the risk-informed, performance-based activity selection approach described in Section 1.4.1, changing seepage enhancing conditions due to drift degradation or focusing of flow because of residuals from thermal processes (e.g., plugging of fractures or enhanced flow through fractures activated by thermal-mechanical processes) were judged to be significant. There is confidence that the modeled range of the rock-mass moisture content, fracture permeability, and perturbed thermal effects will not be exceeded. A change in these rock water parameter values, greater than that currently used as the range in the performance assessments, would change the selected conceptual models or require consideration of additional conceptual models. For the above reasons, this activity is important. In addition, the near-field environment is important to evaluating the performance life times of the Engineered Barrier System components, as well as the drift stability after heating and cooling. For the reasons presented* *above, this activity is designed to meet the requirements of 10 CFR 63.131(a)(1) and (2), 10 CFR 63.132(a), (b), (c), and (e); and 10 CFR 63.133(a).* " [14, p. 3-42]

The stated confidence in the validity of range of the perturbed thermal effects is baseless, as described in the foregoing regarding relative humidity and condensation film-triggered in-drift induced thermal-hydrologic seepage, reported in 2008 Nye County [16, Exhibit 1]. This seepage component fundamentally changes the flows in the near-field rock mass. The three thermal tests that are listed to support current understanding [14, p. 3-43] miss the opportunities for gaining a better understanding of the processes. Three examples for missed opportunities in past activities are: (1) the heat balance mismatch at Drift-Scale Test (DST) evaluations; (2) the moisture balance mismatch at DST; and (3) the lack of explanation for the sign of rust spot on the drum heaters as shown in Exhibit 2 of the report [16, Exhibit 1]. All three observations were explained by uncertainties within the expected range of parameter variations. However, thermally-induced seepage is not considered, nor planned to be monitored.

Seepage monitoring is inadequately planned. The planned activity only *" evaluates the expected results of the liquid infiltration, unsaturated zone flow in the rock above the repository, and seepage into the drift models."* [14, p. 3-20]. These elements are all rated as ITWI (Important To Waste Isolation) in the S*afety Analysis Report*. [15, Table in p. 2.1-3]. However, thermally-induced seepage is not considered, nor planned to be monitored.

The selection for justification states: " *Based on results from the risk-informed, performance-based activity selection approach described in Section 1.4.1, there is confidence that the modeled range of this parameter will not be exceeded and that a change in the parameter value greater than that currently used as the range in the performance assessments would likely change the selected conceptual models or require consideration of additional conceptual models. Therefore, this activity evaluates the seepage assumptions and expected values. This long-term field collection activity provides a direct measurement of seepage quantity and chemistry if present and able to be sampled.* " [14, p. 3-20].

This statement contradicts our model results and even that of DOE stating that " *Underground openings in unsaturated rock divert water around them because of the capillary barrier effect. Therefore, much of the water that percolates downward through the Yucca Mountain unsaturated zone will not seep into the drifts or reach Engineered Barrier System components. <u>However, it is possible for the water potential in the rock formation to be higher than at the drift wall. When this occurs, water will exit the formation and enter the drift. At the drift surface, water can: (1) evaporate, (2) be transported as film flow down the wall, or (3) form a drop that eventually detaches becoming drift seepage. The impact of heat, generated by the decay of radioactive wastes, on drift seepage is of special interest.</u> [emphasis by authors of this report] The hydrological and mechanical alteration of the rock physical parameters (i.e., permeability, porosity, moisture content, fracture interconnectivity) and the chemical evolution of waters, gas, and minerals are coupled to the thermal loading. Zones of boiling, condensation, and drainage are expected to influence the seepage distribution and water chemistry.* " [14, p. 3-21). The facts are known, see emphasized, underlined text above, yet no PC activities are planned to monitor and verify such processes.

The current understanding in Section 3.3.1.2 of SNL 2008a is fragmental as explained in the foregoing regarding relative humidity and condensation water film triggering effect. The anticipated methodology in point 3.3.1.2 does not address the boundary parameter effects on seepage. Seepage monitoring in thermally accelerated drifts is meant to *"test the impact of decay heat on drift seepage."* [14, p. 3.22]. It should be the impact of relative humidity and in-drift condensation that need to be tested, not decay heat. The document lists only problems but not solutions: " *However, the high-temperature and high-radiation environments representative of postemplacement conditions in the thermally accelerated drifts will require development of applications for the technology capable of remote monitoring. Experience gained in thermally accelerated drift tests may contribute to developing technologies for such applications. Revisions to the Performance Confirmation Plan will update this activity description, as appropriate.* "[14, p. 3-22 and p.3-23].

Further reference is given to Section 3.4.5 regarding the thermally accelerated drift concept, undeveloped at this time [14, p. 3-87 and p. 3-88]. There are two main deficiencies:

(1) The lack of viable plan to conduct the necessary confirmation activity regarding in-drift induced thermal-hydrologic seepage. Influencing parameters neglected to date will be difficult if not impossible to evaluate by remote measurement means under radiation conditions. The induced seepage will be mixed with the condensates and it will be impossible to quantify the induced seepage component. The difficulty of the chemical components will be a function of the mixing rate of seepage and condensation, an unknown parameter itself.

(2) The lack of controlled experiments that can verify seepage for post-closure application. During a small set of emulated would-be experiments during pre-closure cannot be rated adequate. The measurement data from accelerated measurements obtained during pre-closure in emulated post-closure settings does not provide the intended purpose of performance confirmation for correct process models for post-closure performance.

As stated in the performance confirmation plan, "*There is no intended requirement regarding performance confirmation methodologies in the PC plan.*" [14, p. 2a]. However, a doable plan has to be presented in the PC activities regarding the understanding of seepage for post-closure performance analysis.

1.1.4 Thermally accelerated in-drift environment monitoring

This activity as planned lacks the quantification and validation of thermo-hydrologic seepage that enters the emplacement drift.

The purpose and justification for this activity are as follows: "*The purpose of this activity is to evaluate assumptions used in in-drift physical and chemical environment models. Characterization of the environment that surrounds the waste package container and drip shield supports evaluating the performance life times of these Engineered Barrier System components. The major degradation mode that can affect the performance of these components is corrosion, and the kinds of corrosion and the rates of corrosion are dependent on the environmental conditions that will be measured in this activity."*

"Selection Justification–Because confirmation of the environment that immediately surrounds the Engineered Barrier System components is important for evaluating the performance life times of these components (the kinds of corrosion and the rates of corrosion are highly dependent on the environment), this in-drift environment monitoring activity is important." [14, p. 3-50].

Due to the missing components in the plan, i.e., in-drift process-triggered thermal-hydrologic seepage, this in-drift environment monitoring activity is rated important, but not for the annual dose calculations: " *Based on results from the risk-informed, performance-based activity selection approach described in Section 1.4.1, it is estimated that it is unlikely that the* *mean annual dose calculations would change if these parameter values are found to lie outside its current modeled range, possibly with the exception of the laboratory testing for water conditions (thin films, including microbial effects).* " [14, p. 3-50].

Immediate contradiction is provided in the same section: "*In addition, if the range was exceeded, a change in these parameter values, including the microbial types and amounts, greater than that currently used as the range in the performance assessments, would likely change the selected conceptual models or require consideration of additional conceptual models. As such, if the results of this activity are not as anticipated, the implications on system performance could include a greater potential in the waste package corrosion failure mode and accordingly, a greater potential for Engineered Barrier System breach and radionuclide release to the Lower Natural Barrier.* " [14, p. 3-50, 3-51].

Due to internal contradiction, and due to omitting water/brine seepage monitoring from the in-drift environment, and omitting the monitoring of the basic in-drift processes that contribute to thermal-hydrologic seepage (i.e., air re-circulation and axial heat and vapor transport), this activity is inadequate.

The performance confirmation plan as presented lacks the purpose of "*the condition of the waste packages be monitored against design assumptions*" for any number of emplacement drifts that will include a combination of above and below-boiling temperature regimes, such as presented in the license application.

Based on the presented performance confirmation plan regarding the in-drift induced thermal-hydrologic seepage, it will be impossible to fulfill the important goal as to: *"Report significant differences between expected results and monitoring and testing information to the NRC, along with an evaluation of the effect of those differences on repository design or performance. Such evaluations can include recommended changes to construction methods, design, or performance analysis approaches."* [15, p. 4-5]

1.2 Suggested Remedial Actions

a) A new, coupled process model will be needed to explain the evolution of the coupled, in-drift and near-field thermal-hydrologic processes and their effects on seepage. Such a model can be conveniently constructed using already qualified model-elements developed under Yucca Mountain procedures. The model has to have (1) a CFD component for the in-drift domain, (2) a porous-media model component for the near- and far-field rock domain; (3) adequately fine descritization in the near-field for seepage modeling; and (4) coupling between elements (1) through (3). The new model must be used for the explanation of the performance confirmation measurements and observations. Such a model has been developed and used under Nye County support, reported herein.
b) Revision of the current thermal-hydrologic seepage abstraction will be needed, adding as a new component, in-drift induced thermal-hydrologic seepage abstraction to the TSPA studies. This revision will change the abstraction of thermal-hydrologic seepage from a downward interpolation of ambient seepage (at above-boiling, randomly-spread locations) to induced thermal-hydrologic seepage, to be an upward interpolation of ambient seepage (at below-boiling, focused and fixed locations). Orders-of-magnitude differences between thermal-hydrologic seepage and induced thermal-hydrologic seepage are expected. Then use these expectations in the transport models, corrosion models and dose rate estimates, and in the performance verification activities to increase confidence

that the new induced thermal-hydrologic seepage abstractions are not exceeded during accelerated heated experiments.

c) A new performance confirmation activity will be needed which deals with the confirmation of the coupled in-drift and near-field processes including induced thermal-hydrologic seepage in the cold drift section of an emplacement drift having above-boiling temperatures at the same time.

d) A modified operation plan may be needed pending on the findings in actions (a) through (c) to avoid the development of unfavorable storage environment, possibly reducing the maximum operating temperature to near-or below-boiling in order to eliminate unwanted, coupled processes from occurring, such as induced thermal-hydrologic seepage.

2. Task 2 –Modeling and assessment support for Nye County contentions

2.1. Numerical Studies with MF 5.0

Basic studies were performed first, comparing results corresponding to model assumptions used by DOE to those using more realistic model assumptions, all within the MF model methodology for consistency. These study cases A through C will be published soon in an upcoming Journal of Nuclear Technology paper [11]. Case A refers to Model Arrangement 15 in Table 1, a constant dispersion case of 0.1 m^2/s. Case B refers to Model Arrangement 11 in Table 1, a convective model using the line-load waste package heat generation. Case C, corresponding to Model Arrangement 14, a dispersive model with the new variable axial dispersion coefficient along the drift obtained from Case B using the vapor/moisture flux matching method. In all Cases A through C, the unheated section is 80 m at both ends with symmetrical arrangement.

In this section, first the main model concept, solution technique and model domains are explained followed by the comparison between Case A, through Case C.

2.1.1 Model Concept

The numerical simulator MF Version 5.0 is used in the evaluation of three different in-drift transport approaches, each utilizing different transport mechanisms. The coupled in-drift airflow field, caused by natural convection, is explicitly and iteratively solved within MF, using its three-dimensional integrated-parameter solver for the Navier-Stokes equation. The natural air flow field is simultaneously used for a direct simulation of the axial heat and moisture fluxes. The WPs are modeled as individual heat sources at with an initial line load of 1.45 KW/m along the heated section of the emplacement drift. The initial load decreases exponentially with time as a result of radioactive decay. During the 50-year pre-closure period following waste emplacement, forced ventilation removes the majority of the heat from the repository, ensuring that the temperature increase is moderate and access to the drifts is still possible.

2.1.2 Thermal-hydrologic Model of the Rockmass

The rockmass surrounds a representative drift in the middle of an emplacement panel. The various model domains are shown in Figure 2-1. The length of the drift is 760 m with two 60-m and 15-m long end sections where no waste is emplaced. The unheated drift sections are connected to the undisturbed and also unheated edges, which provide a dominantly conductive heat sink to the heated portion of the rockmass around the center of the emplacement drift.

Likewise, the representative NTCF model, a surrogate model using response functions based on the TOUGH2 thermal-hydrologic porous-media code, is also used unchanged.

Along the length of the drift, 48 individual mountain-scale divisions are applied. The relationships between the set of input *T*, *P,* and output *qh, qm* temporal variations for each drift section define the corresponding dynamic, rockmass model for heat and moisture according to the following matrix equations[17]:

$$qh = qh^c + hh \cdot \left(T - T^c\right) + \langle T \rangle \cdot hm \cdot \left(P - P^c\right) \quad (1)$$

$$qm = qm^c + mh \cdot \left(T - T^c\right) + \langle T \rangle \cdot mm \cdot \left(P - P^c\right) \quad (2)$$

Where *qh* and *qm* are NTCF output heat and moistures fluxes,

hh and *hm* are NTCF dynamic admittance matrices for heat,

hm and *mm* are NTCF dynamic admittance matrices for moisture,

T is input temperature,

P is input vapor pressure, and

superscript *c* refers to central boundary conditions.

The *hh*, *hm*, *mh*, and *mm* dynamic admittance matrices are identified based on Eqs (1) and (2) by fitting *qh* and *qm* to TOUGH2 data. The NTCF model identification method follows the technique described in [4]. The model for each drift-section perfectly reproduces qh^c and qm^c, the central output fluxes from TOUGH2, for $T=T^c$ and $P=P^c$, the central input boundary conditions.

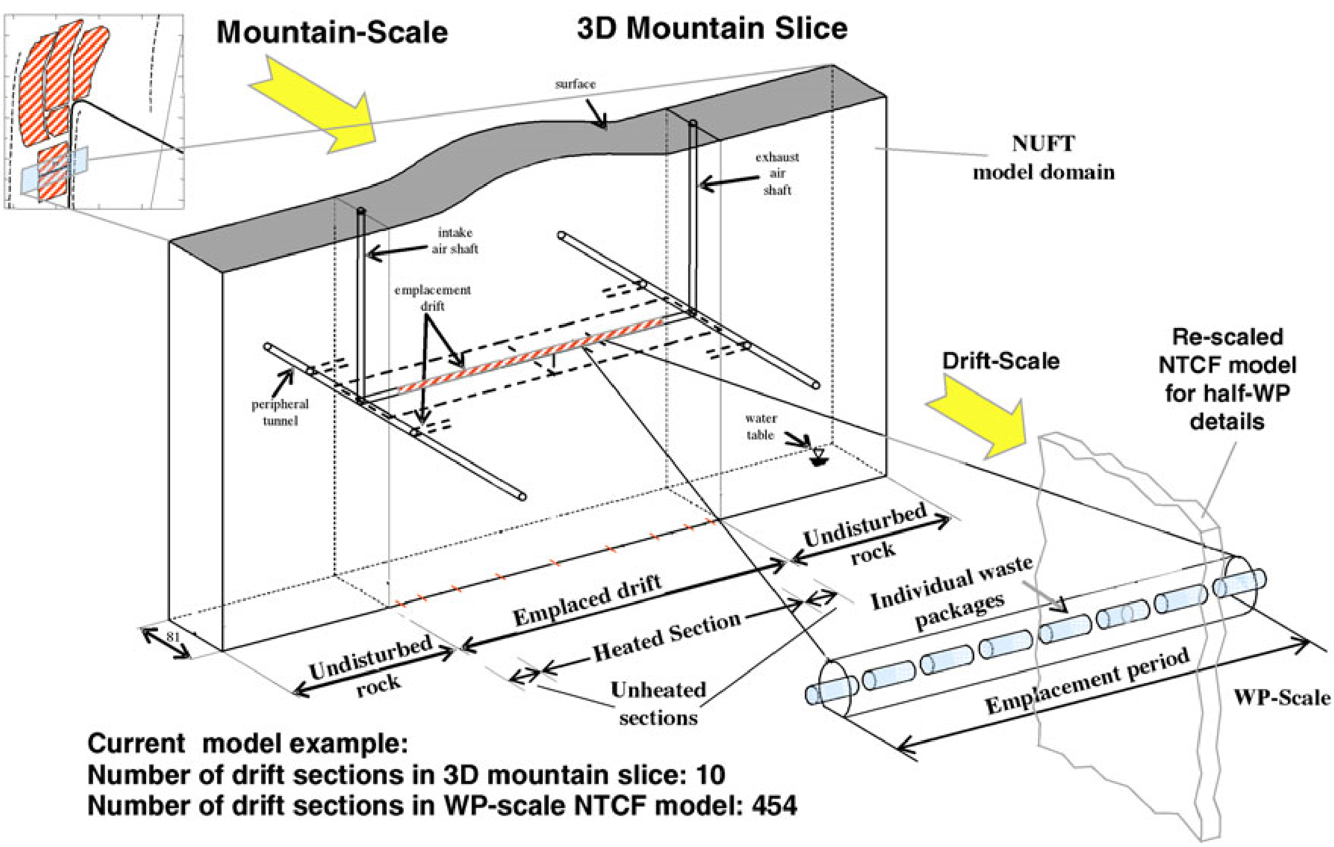

Figure 2-1. Multi-scale, in-rock and in-drift model domains (From Danko, et al., 2008 [18])

Other T and P input variations can produce outputs from the NTCF model for qh and qm without actually re-running TOUGH2. For the coupled in-rock and in-drift model, 454 drift-scale NTCF models are generated from the mountain-scale NTCF models by scaling, following the technique used in [17].

2.1.3 CFD Models for Heat, Moisture, and Air Flow Transport in the Emplacement Drift

The integrated-parameter, in-drift CFD model domain is also identical to that in a previous study [17]. However, the heat, mass, and air flow transport connections within the emplacement drift are configured according to the model approach of Model Arrangement 18 in Table 1.

The energy balance equation in the CFD model of MF is used in a simplified form, as follows, for an x-directional flow with v_i velocity in a flow channel of cross section dy by dz (and with no convective heat transport in y and z directions while considering the x-directional flow):

$$\rho c\frac{\partial T}{\partial t}+\rho c v_i\frac{\partial T}{\partial x}=\rho c a\frac{\partial^2 T}{\partial x^2}+\rho c a\frac{\partial^2 T}{\partial y^2}+\rho c a\frac{\partial^2 T}{\partial z^2}+\dot{q}_h \tag{3}$$

In Eq. (3), ρ and c are density and specific heat of moist air, respectively; a is the molecular or eddy thermal diffusivity for laminar or turbulent flow; and $\dot{q}_h$ is the latent heat source or sink for condensation or evaporation. In this model, a equals the molecular diffusivity in all directions, as moisture transport by convective air flow is explicitly modeled. The second and the third terms on the right-hand-side of Eq. (3) represent heat conduction (or effective heat conduction) in the y and z directions, normal to the x axis of the flow channel; these terms are substituted with expressions for transport connections using heat transport coefficients for flow channels bounded by solid walls. Eq. (3) is discretized and solved numerically and simultaneously along all flow channels for the temperature field T in MF [19].

The simplified moisture transport convection-diffusion equation in the CFD model of MF is similar to Eq. (3) as follows:

$$\rho\frac{\partial \omega}{\partial t}+\rho v_i\frac{\partial \omega}{\partial x}=\rho D\frac{\partial^2 \omega}{\partial x^2}+\rho D\frac{\partial^2 \omega}{\partial y^2}+\rho D\frac{\partial^2 \omega}{\partial z^2}+qc+qs+qm \tag{4}$$

Where ω is the vapor mass fraction $\omega=\dfrac{P\cdot Ra/Rv}{Pb-(1-Ra/Rv)\cdot P}$

x, y, z are Cartesian coordinates,
t is time
P is partial vapor pressure,
Pb is air total, barometric pressure,
Ra is gas constant for dry air,
Rv is gas constant for water vapor,
ρ is density of moist air,
D is the molecular or eddy diffusivity for vapor for laminar or turbulent flow,
qc is the moisture source or sink due to condensation or evaporation at node i, and
qs is the vapor flux source or sink at node i in superheated steam form.

D is calculated from the thermal diffusivity, a, which is substituted specifically according to as explained for Eq. (3).

The Navier-Stokes momentum balance equation for 3D flow of the bulk air-moisture mixture is used as follows, following [20]:

$$\rho\left(\frac{\partial v_x}{\partial t}+\mathbf{v}\cdot\nabla v_x\right)=\rho g_x-\frac{\partial Pb}{\partial x}+F_x \tag{5a}$$

$$\rho\left(\frac{\partial v_y}{\partial t}+\mathbf{v}\cdot\nabla v_y\right)=\rho g_y-\frac{\partial Pb}{\partial y}+F_y \tag{5b}$$

$$\rho\left(\frac{\partial v_z}{\partial t}+\mathbf{v}\cdot\nabla v_z\right)=\rho g_z-\frac{\partial Pb}{\partial z}+F_z \tag{5c}$$

Where v_x, v_y, v_z are velocity components of vector v,

g_x, g_y, g_z are gravitational forces which include buoyancy in x, y, and z directions, and

F_x, F_y, F_z are viscous terms.

The viscous terms in Eqs. (5a-c) are expressed with the viscous normal-stress $(\sigma)_v$ and shear-stress (τ) components as follows [20]:

$$F_x=\frac{\partial(\sigma_{xx})_v}{\partial x}+\frac{\partial\tau_{yx}}{\partial y}+\frac{\partial\tau_{zx}}{\partial z} \tag{6a}$$

$$F_y=\frac{\partial\tau_{xy}}{\partial x}+\frac{\partial(\sigma_{yy})_v}{\partial y}+\frac{\partial\tau_{zy}}{\partial z} \tag{6b}$$

$$F_x=\frac{\partial\tau_{xz}}{\partial x}+\frac{\partial\tau_{yz}}{\partial y}+\frac{\partial(\sigma_{zz})_v}{\partial z} \tag{6c}$$

The viscous force terms in Eqs. (6a-6c) are integrated along the grid lines of the flow channels and expressed as a function of the convective air flow components in the emplacement drift [17].

The integrated-parameter CFD model approach allows for reducing the number of discretization elements in the computational domain. MF allows for defining connections between integrated volumes, applying direct heat and moisture transport relations between them. The current, integrated-parameter CFD model in the drift applies 18x454=8172 nodes for the heat, and the same number of nodes for the moisture transport as well as for air flow transport. Each WP is represented by two nodes, with one additional node for the gap between neighboring containers. CFD nodes are in the airway along four longitudinal lines in a half-cross-section of the drift on either side of the symmetry line: (1) close to the floor; (2) close to the drip shield; (3) close to the drift wall at mid-height; and (4) above the drip shields, with 454 nodes on each line. The drift wall is assumed to be separated from the rock with a 10^{-5} m-thick still air layer representing the rock-air interface, and acting as a coupling layer of insignificant resistance to transport of heat and moisture. Both the drift wall and the thin coupling layer are represented by 454 nodes each along three longitudinal lines along the drift length: at the invert, sidewall, and roof. The airspace under the drip shields is also modeled by four lines, each having 454 nodes. Half of the drip shield on either side of the symmetry line is represented by four nodes defining four lines, two on the top and two on the side. Each air space, one above and one under the drip shield, also includes one steam transport line. Heat and moisture transport are modeled using heat and moisture transport coefficients at the WP, drift wall, and at each side of the drip shield. 3D thermal radiation between solid surfaces is also included in the CFD model.

Natural air flow is considered due to the local temperature differences in the vertical planes normal to the drift axis. The radial, tangential, and axial velocity components are all explicitly modeled and calculated in MF.

2.1.4 Coupled In-rock NTCF and In-drift CFD Models

The NTCF (approximating the rockmass response) and CFD models are coupled on the rock-air interface by MF until the heat and moisture fluxes are balanced at the common surface temperature and partial vapor pressure at each surface node and time instant. Two iteration loops are used to balance the in-rock and in-drift transport processes on the rock-air interface:

1. Heat flow balance iteration between the NTCF and airway CFD models for each time division.
2. Moisture flow balance iteration between the NTCF and airway CFD models for each time division.

An outer iteration loop is used to determine the natural air flow field in the closed air space of the emplacement drift. For each set of balanced results from iterations 1 and 2, the air flow velocity field is solved based on the new, updated temperature and vapor pressure distribution in an outside balance loop until no significant change is observed between consecutive iterations. The convergence of the iteration for the velocity distribution in the natural air flow field is discussed in another paper [9]. Suffice to recite that it is no small accomplishment to make this iteration converge, considering that the result is the solution of a set of nonlinear equations with several thousands of unknown variables.

The simulation results obtained from the CFD model elements are temperature, relative humidity, and water condensate variations within the emplacement drift, including their distributions on the drift wall boundary. Relative humidity is defined as the ratio of partial vapor pressure, P, to barometric pressure, Pb. In the current study, we focus on these in-drift conditions. In other studies, the main focus may be directed to the processes in the rockmass and not in the drift, such as in [5, 21]. Temperature, humidity, and moisture flow distributions in the rockmass, already coupled to the in-drift processes, are given by the TOUGH2 porous-media model. Read-out of saturation and/or moisture flow results in the rockmass from TOUGH2 at any time instant can be made during the MF runs at the end of a successful iteration for heat and moisture flow balances.

The CFD model configuration in the convective model eliminates the need for the equivalent dispersion coefficient, and thus offers several advantages. First, the dispersion coefficient is a flow, and not a fluid property, a time- and spatial-dependent function which varies from case-to-case. Second, only limited dispersion coefficient data are available in the YM literature for the drift air space [3]. Third, there is no efficient method in sight other than solving first for real convection and post-processing the results to supplement dispersion coefficients for future model studies with various, new boundary and flow conditions in various emplacement drifts in any given emplacement panel at YM.

2.1.5 Analysis of axial dispersion vs. convection

The analysis of axial dispersion vs. convection relevant to transport models in an emplacement drift at YM relates to the baseline models used for predicting in-drift environment. A new dispersive model has been developed and tested which will provide an improved match between a simplified, dispersive model such a used by Birkholzer [5] and Buscheck [1] and the convective model used by Nye County in terms of temperature, vapor pressure, and flux distributions. It is also expected that the scientific basis will be ignored regarding the in-drift axial transport mechanism approximated by equivalent dispersion in the YM baseline models.

Case C is based on a dispersive model with the new variable axial dispersion coefficient along the drift obtained from Case B using the vapor/moisture flux matching method at each WP location, described in March 2009 report [22].   Figures 2-2 through 2-6 show the axial dispersion coefficients for half of the drift length. The raw values and the ones obtained from the semi-empirical curve fitting are shown together for inside and outside the drip shield at selected post-closure time periods. The smoothened values were used in the dispersive model of Case C.

Figure 2-7 shows comparison of temperature between Cases A, B, and C for a few time divisions. Figure 2-8 shows comparison of relative humidity distributions. In-drift condensation comparison is shown in Figure 2-9. Dispersion can be a good replacement for convection regarding temperature distributions since good agreement is found between cases B and C. The agreement is somewhat poorer for humidity and condensations. However, the results showing good agreement in Figures 2-7 through 2-9 refer to an equivalent dispersion coefficient about 40 times higher than the highest values used in DOE's models and in the LA documents. An order of magnitude difference in the axial dispersion coefficient is a serious disagreement regarding the highest reported value. Even more serious is the disagreement between the highest dispersion coefficient value used in the LA models (0.025 m^2/s) and the new results. The comparison between the range of the effective dispersion coefficients is shown in Table 1-1.

Table 1-1. Range of the equivalent, effective coefficient in the emplacement drift.

Highest D_{eff} in the LA thermal-hydrologic models	Highest D_{eff} reported in the LA	Peak D_{eff} back-calculated from the convective model in the present studies
0.025 m^2/s	0.1 m^2/s	1.0 m^2/s

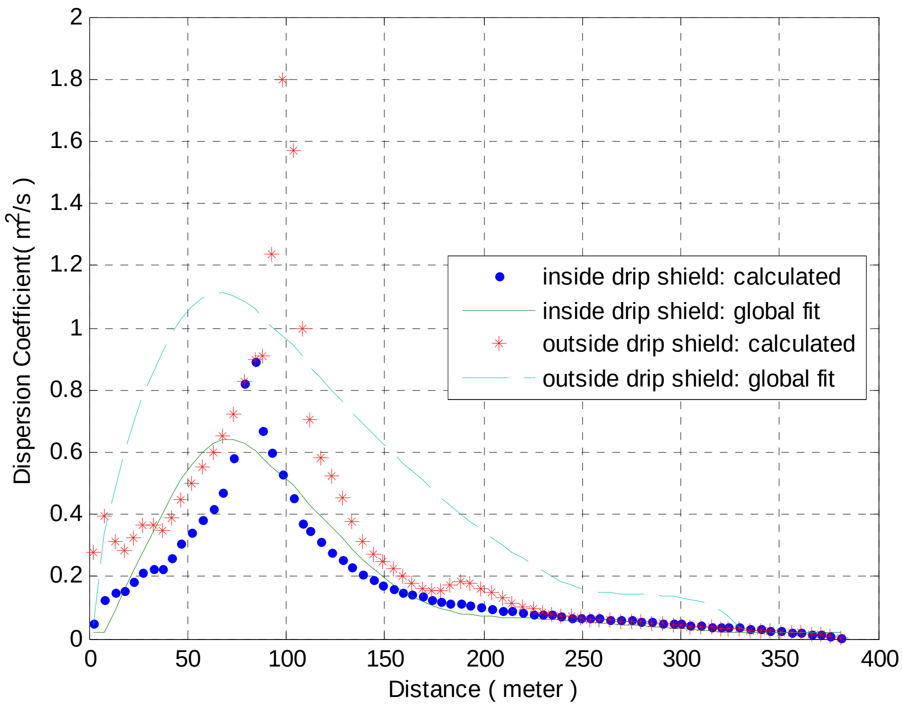

Figure 2-2. Axial dispersion coefficient distribution at Year 51.

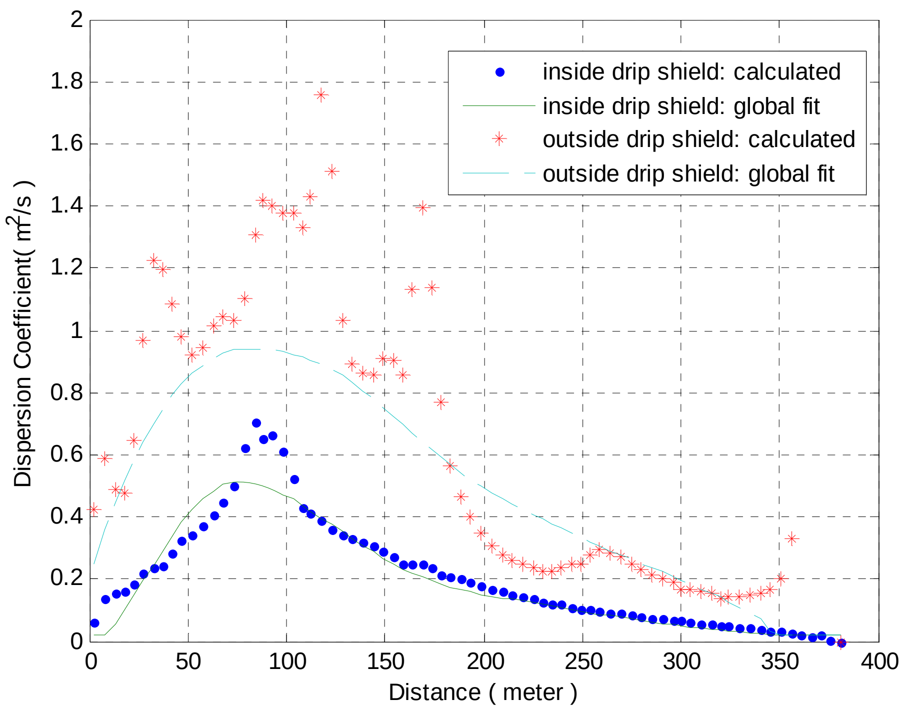

Figure 2-3. Axial dispersion coefficient distribution at Year 75.

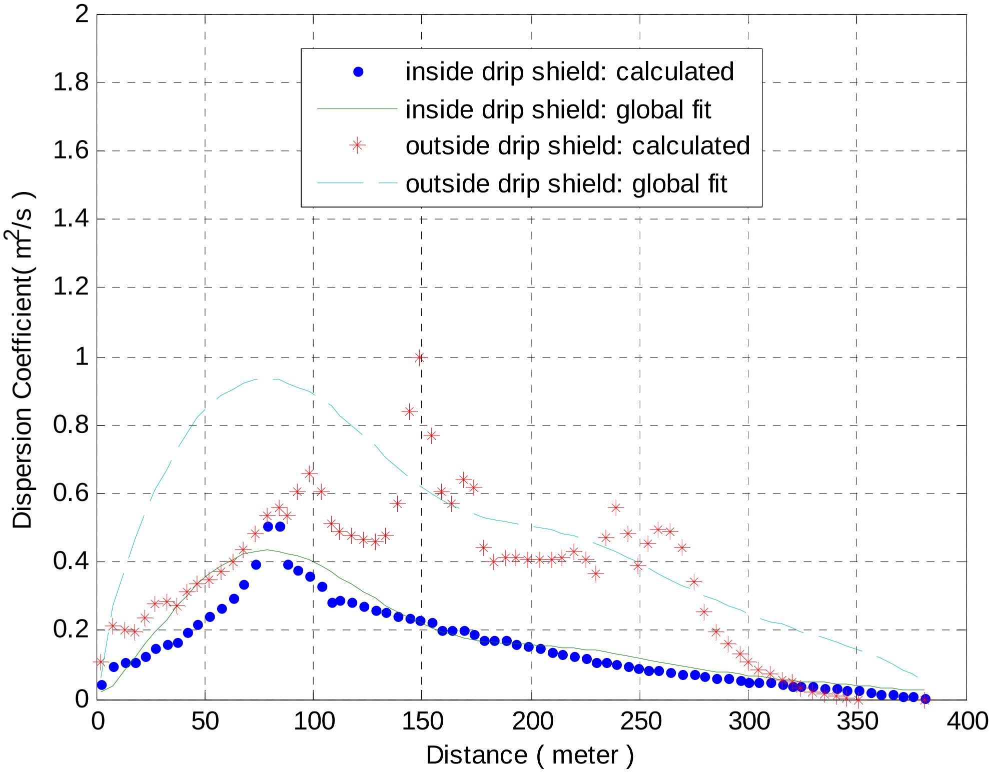

Figure 2-4. Axial dispersion coefficient distribution at Year 300.

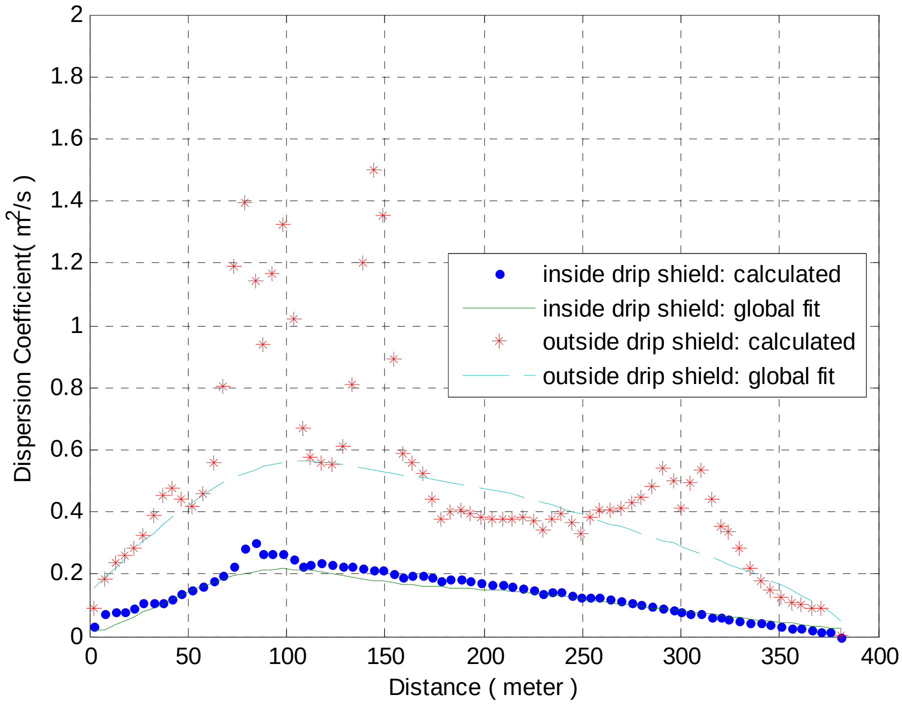

Figure 2-5. Axial dispersion coefficient distribution at Year 1000.

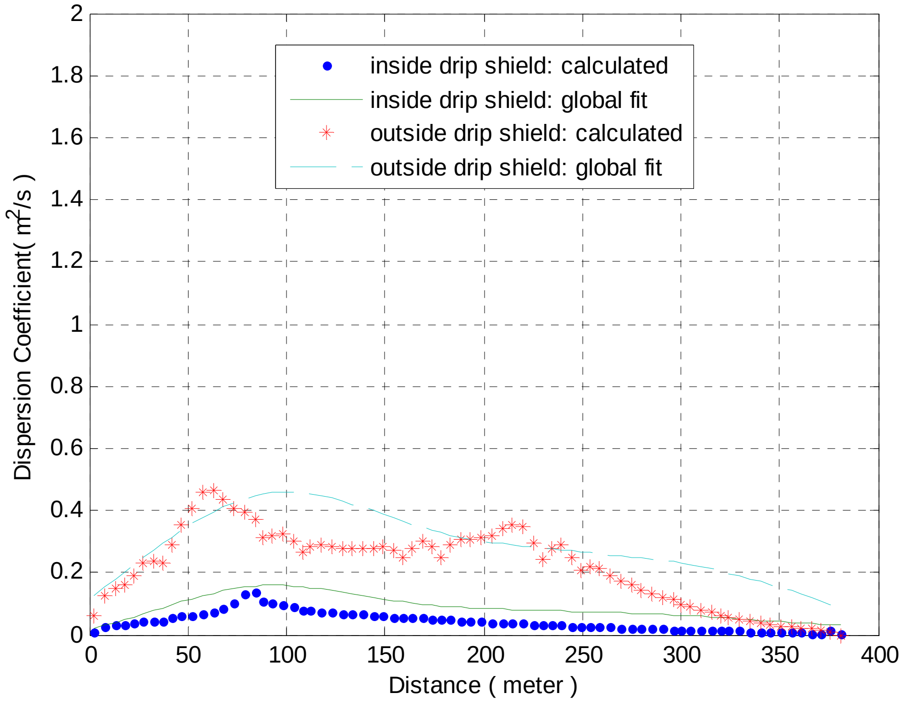

Figure 2-6. Axial dispersion coefficient distribution at Year 5000.

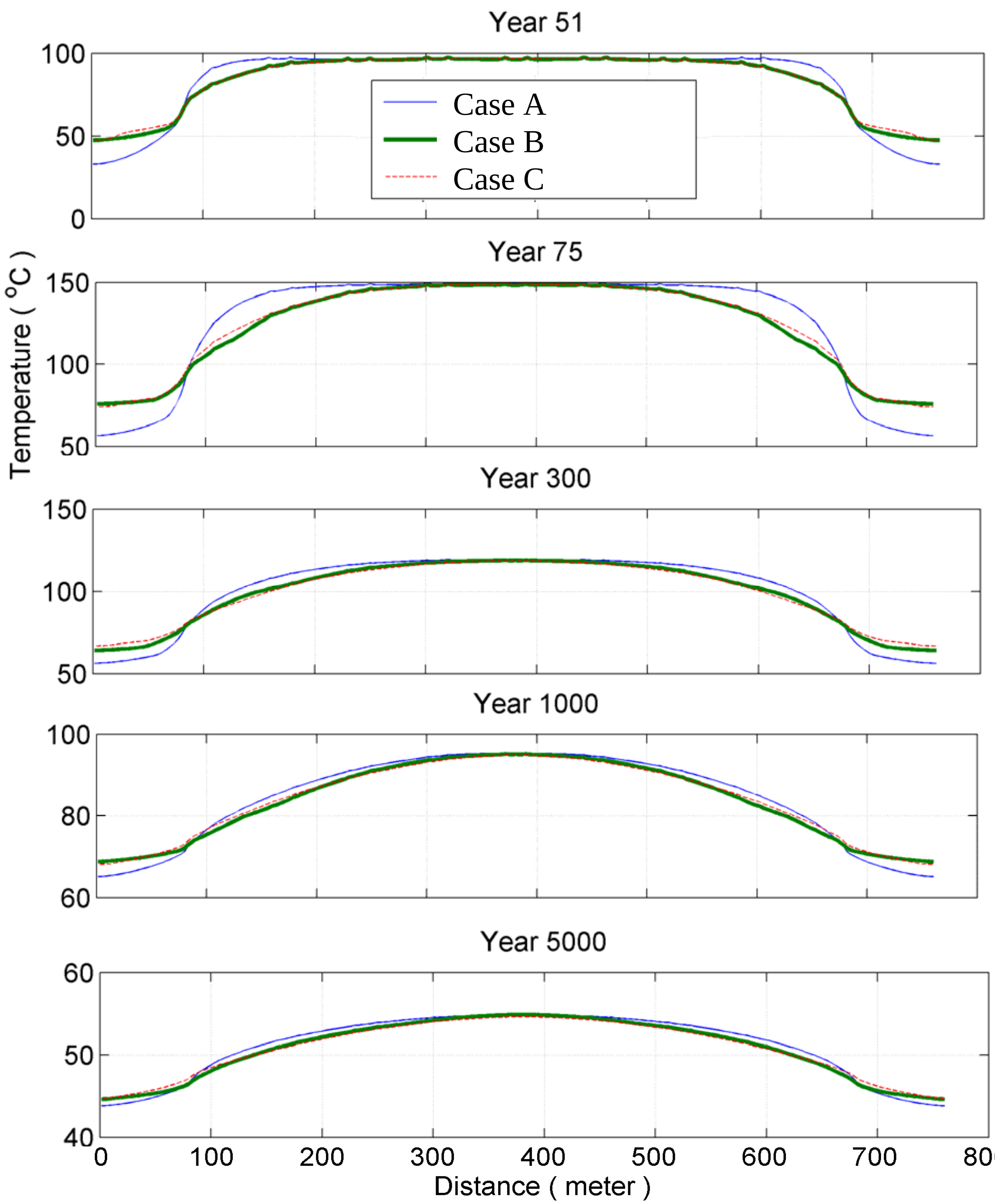

Figure 2-7. Drift invert temperature variation with drift length at selected post-closure time periods.

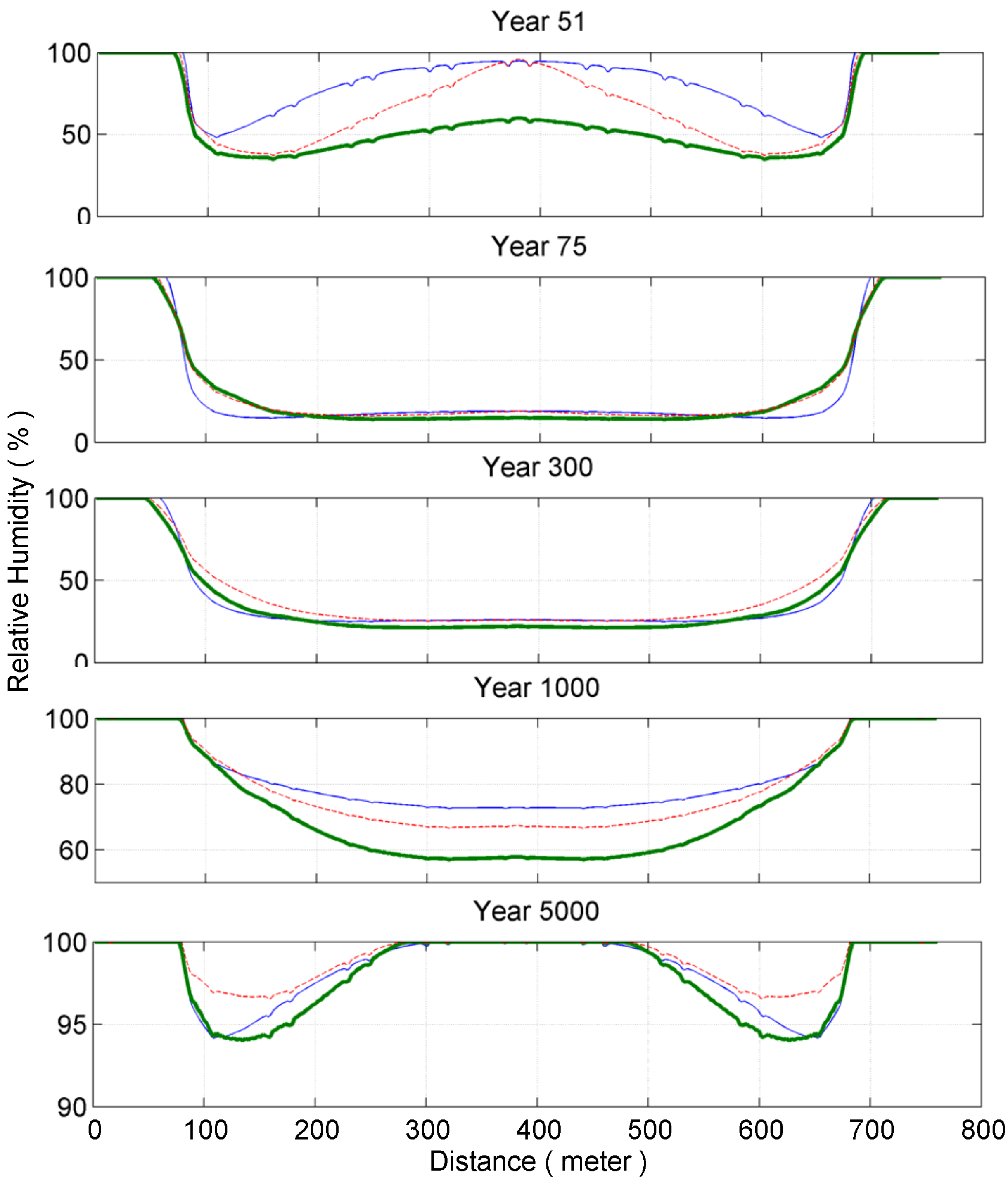

Figure 2-8. Drift invert relative humidity variation with drift length at selected post-closure time periods.

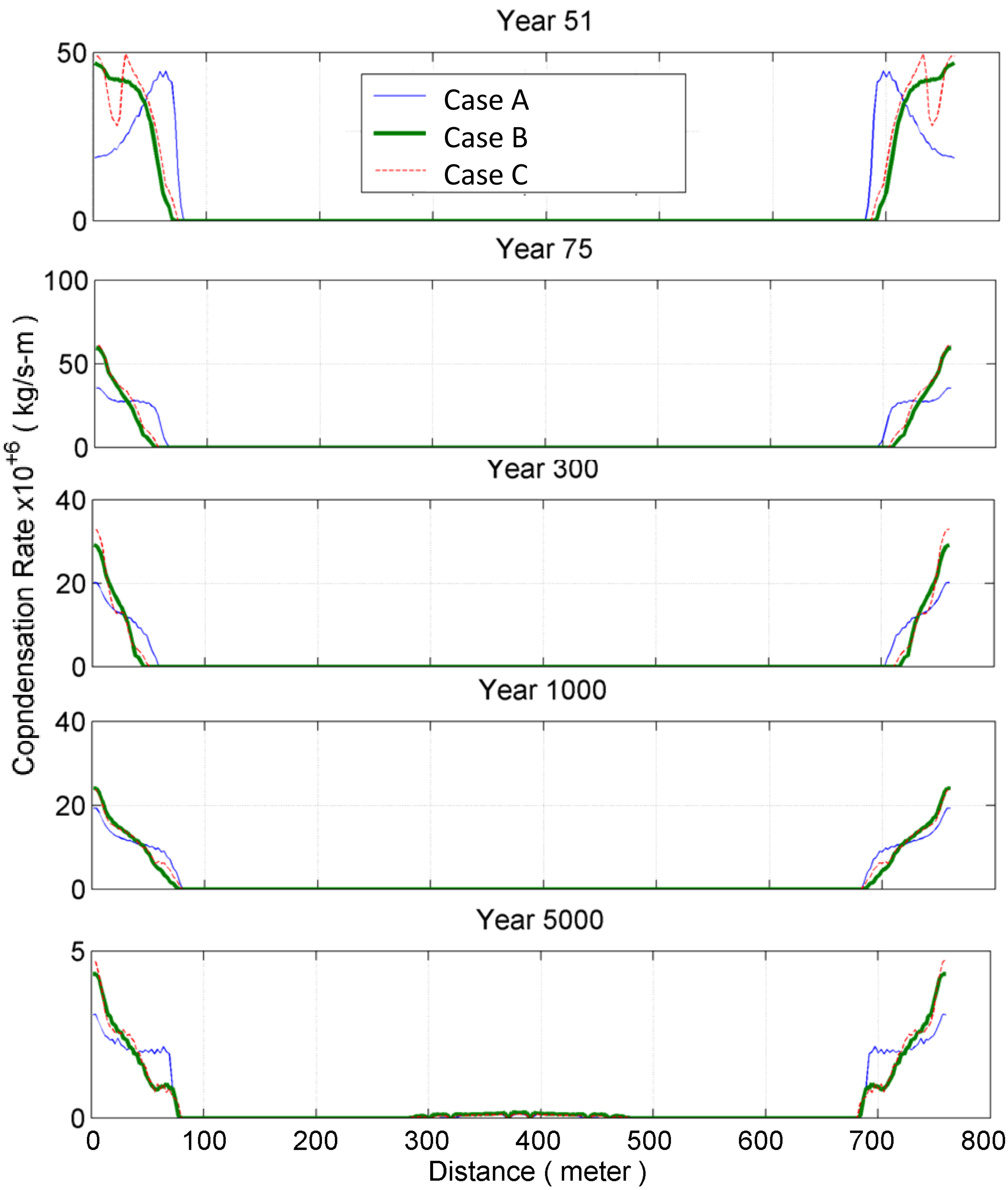

Figure 2-9. Drift condensation flux variation with drift length at selected post-closure time periods.

2.2. Comparison between the LA and Nye County models

In order to resolve the question on the validity of the MSTHM model in the LA, the partial results of three other models are reported here. The model domain and components are the same as described in the previous section. The unheated drift lengths are set to 60-m and 15-m according to the LA design geometry from cases A through C. A major improvement relative to the models in cases A through C is the application of an automated Outside Balance Iteration (OBI) cycle that refines the NTCF model iteratively against many TOUGH2 runs during the MF model calculations.

There are further variations in the input parameters and model conditions. The first case, referred to as "diffusive model", assumes only molecular diffusion in axial direction (no dispersion enhancement is used in this case). This case re-models the MSTHM, which assumes no dispersion enhancement factor in the LA (Model arrangement 23 in Table 1). The model configuration and start of balancing calculations were reported in the June 2009 Progress Report.

The second case, referred to as "dispersive model", is used to check the validation case for omitting axial transport by DOE in the LA models, based on the MSTHM report. The dispersive model applies a dispersion coefficient set to 1000 times the air molecular diffusion due to axial convection-enhancement (Model arrangement 22 in Table 1) (a value most justified from the dispersion coefficient study, see cases B and C comparisons) as opposed to a multiplication factor set to only 25 to enhance the air molecular diffusion in the LA model (which low multiplication factor of 25 has absolutely no justification in the LA documents) [1]. The model configuration and start of balancing calculations were reported in the June 2009 Progress Report. Strictly speaking, the LA thermal -hydrologic model used a simplification relative to the LA design. The design assumes asymmetrical unheated sections of 60 m and 15 m, whereas the MSTHM model used zero unheated section lengths at both ends. Our model is closer to the design specifications, making another refinement in the search for realistic results.

The third case, referred to as "convective model", applies the true, coupled convective transport model simulation (Model arrangement 18 in Table 1). The model configuration and start of balancing calculations were reported in the May 2009 Progress Report. The "convective model" is different from the convective model in Case B in Section 2.1, as it is further refined in matching the LA design (asymmetrical unheated section, and variable as opposed to line-averaged heat load) and further refined in the MF 5.0 model execution (a full OBI iteration between MF and TOUGH2, as opposed to using a fixed NTCF-TOUGH2 model for the rockmass).

The in-drift air velocity fields are prepared first from the convective model. The velocity fields are the results of the complete thermal-hydrologic simulation in the drift air space, coupled to the thermal-hydrologic simulation in the rockmass. Therefore, these results implicitly include the temperature and humidity distributions which are also reported.

Figures 2-10 and 2-11 show the axial air velocity variation along the drift length at year 60 for the air space above the drip shield. Figures 2-12 and 2-13 show similar results for the air space under the drip shield. The positive velocity identifies air flow direction from the entrance toward the exit end. The four air lines in each air space (under or over the drip shield) are grouped in two lines. For example, if flows along three air lines go in one direction, they are averaged into one line. The results show large and small air circulation loops. The large loops are long-distance events, while the small ones are formed over a short axial distance. As it can be seen in Figure 2-10, no small air flow loops are present in the air space above the drip shield from year 75. Results for the air space under the drip shield are shown in Figures 2-12 and 2-13. Small circulation loops appear to form easier in the air space over the drip shield.

This circulation behavior is consistent with expectations: a larger space over the drip shields has lower flow resistance and a corresponding high flow reversibility characteristics under small driving force changes. The long, axial circulation loops are responsible for enhanced moisture transport between the hot section and unheated end sections. This is a phenomenon that has been left out from the DOE models entirely. The formation of robust axial air flow loops and their effects in axial heat and moisture transport are played down in the LA studies as insignificant. However, the study of significance in the LA is biased, using far too low of a multiplication factor (25 as opposed to 1000). Transversal air velocity variations along the drift length at selected time periods are shown in Figures 2-14 and 2-15 for the air space above the drip shields, and 2-16 and 2-17 for the air spaces under the drip shields.

Figures 2-18 and 2-19 show axial distribution of drift wall temperature along the heated section in the air space above the drip shield. The results show that prior to year 400 the diffusive (Model arrangement 22 in Table 1) and dispersive (Model arrangement 23 in Table 1) models are similar while they are very different from the convective model results (Model arrangement 18 in Table 1). Large differences are seen in the temperatures variations near the edges of the heated section for all time intervals. Figures 2-20 and 2-21 show drift wall temperatures under the drip shields, i.e., on the footwall of the invert.

Figures 2-22 and 2-23 show axial distribution of relative humidity on the drift wall above the drip shield. The results show that the hot region is generally drier from the convective model compared to the dispersive and diffusive models due to more axial moisture transport. Figures 2-24 and 2-25 depict relative humidity distributions on t he invert drift wall under the drip shields.

Figure 2-26 and 2-27 show the evolution of condensation distributions for the convective, diffusive and dispersive models (Model arrangements 18, 22, and 23 in Table 1) above the drip shields. Figures 2-28 and 2-29 depict the condensation distributions under the drip shields.

Figure 2-30 shows the summary of condensation distributions, depicting the sum of total condensation along the drift length as a function of time for the three different models. Figure 2-30 also gives the total vapor inflow into the drift from the near-field rockamss. As shown, for the first few hundred years, the diffusive and dispersive models condense less than the total due to the weak axial moisture transport to the condensation drainage area in the unheated drift sections. The vapor must leave the closed drift air space in superheated vapor form according to the models. This vapor transport is possible via a minute, rather insignificant total pressure increase which is not modeled in MF. Moisture convection in the convective model, which is the most realistic of all three can, however, remove the moisture from the rock along the drift length without the need for increase in the total pressure, and nearly all vapor inflow is removed by condensation

The results show that the diffusive model provides the least amount of condensation which is due to the high axial transport resistance and the removal of moisture in superheated steam form. The convective model provides a smooth trend until year 600 at which time percolation flux at the surface increases, causing a gradual, pronounced but still smooth change. We consider the smoothness of the curve from the convective model a manifestation of model stability and robustness. Although all three models are solved with the same iteration parameters in MF, it is a pleasing fact that our best, most sophisticated model provides the most stable and reasonable result.

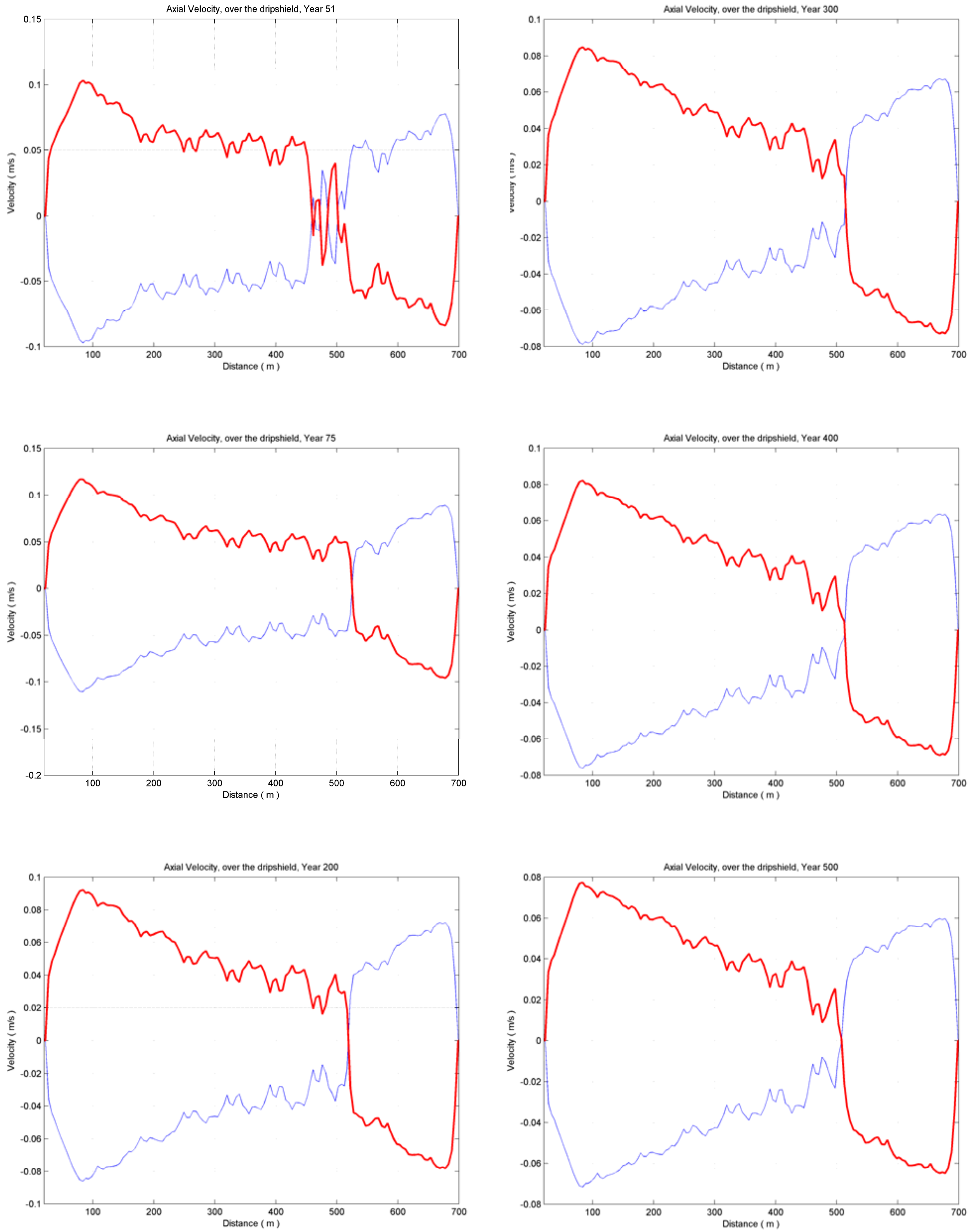

Figure 2-10. Axial air velocity variation above the drip shield at selected post-closure time divisions.

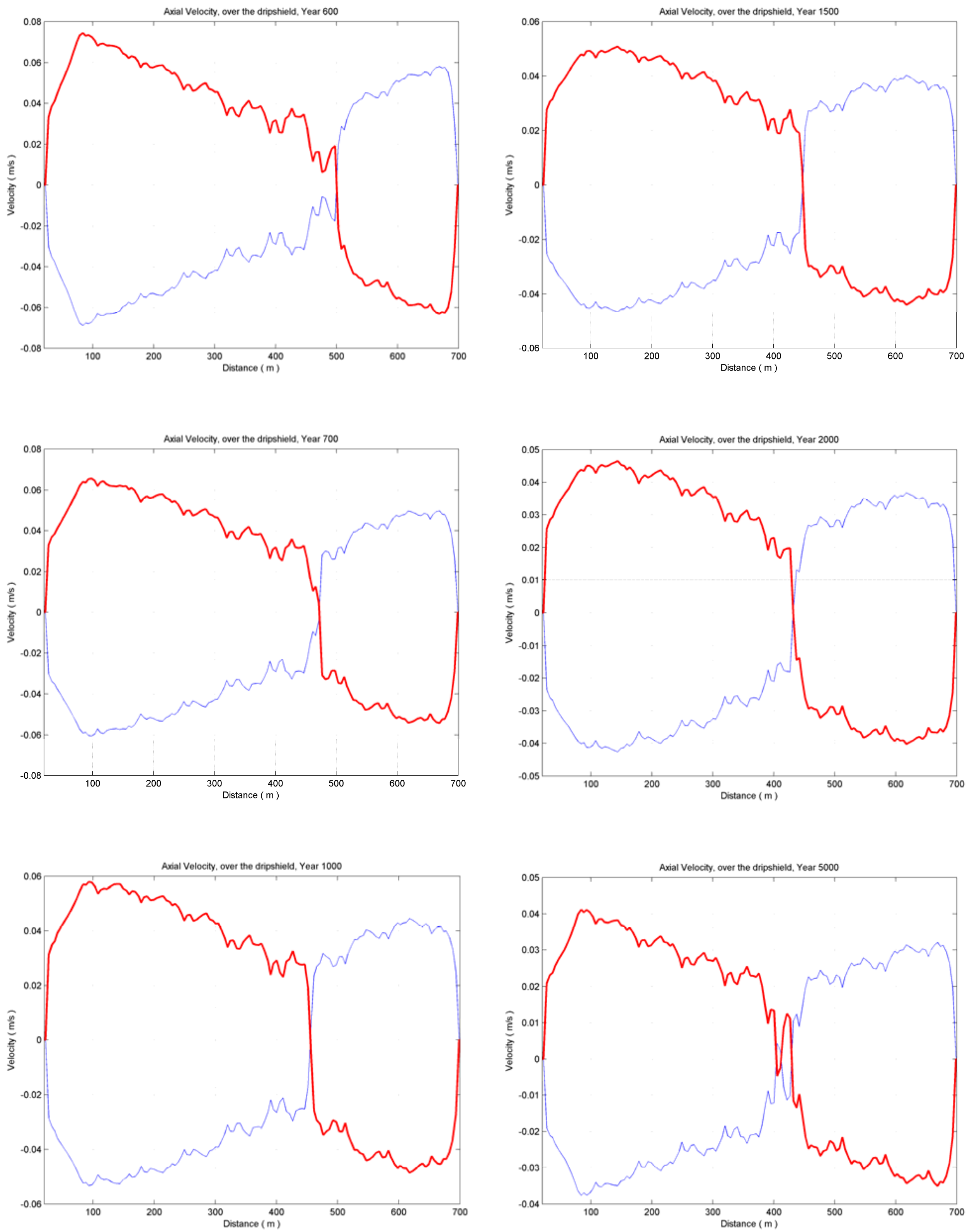

Figure 2-11. Axial air velocity variation above the drip shield at selected post-closure time divisions.

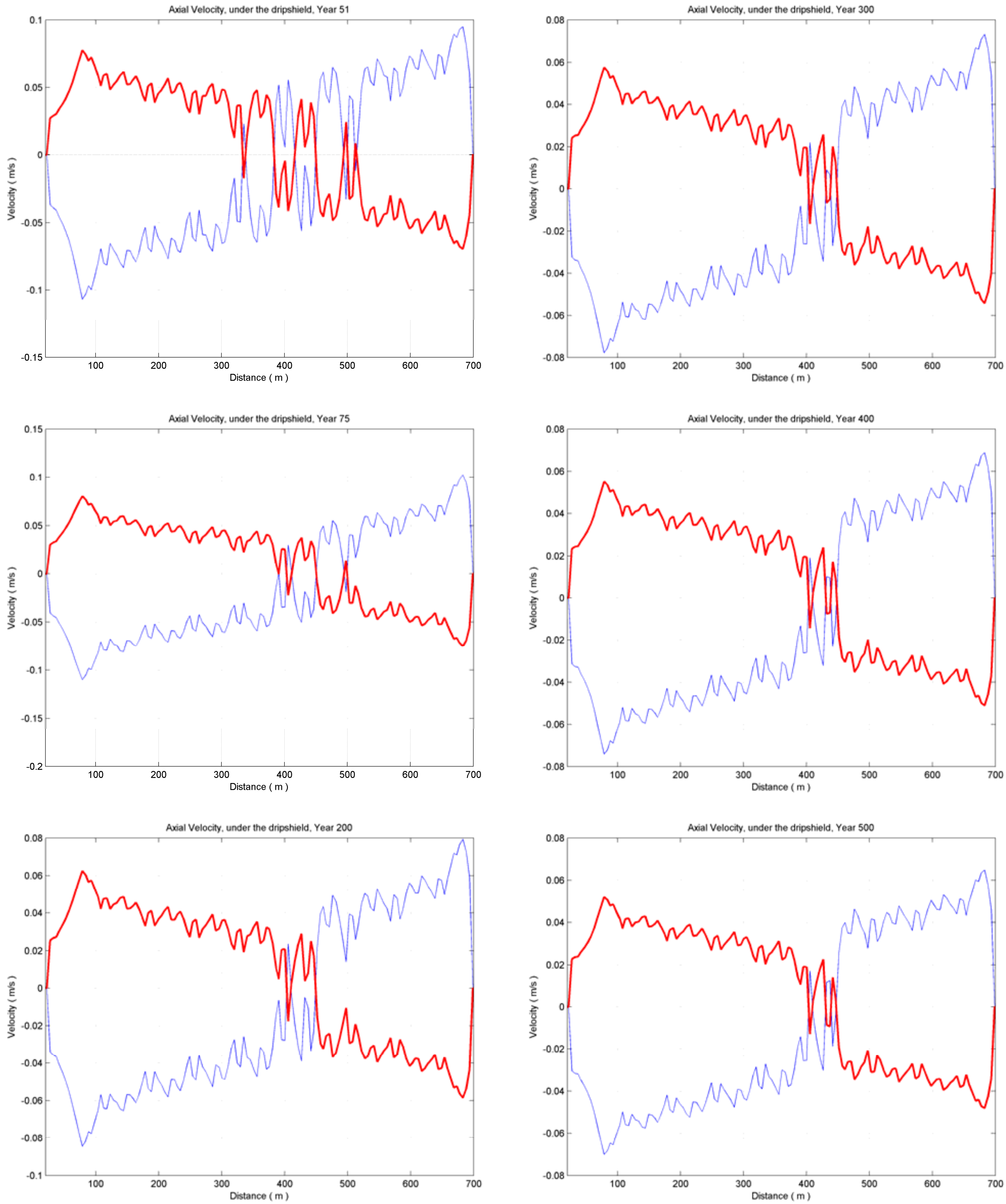

Figure 2-12. Axial air velocity variation under the drip shield at selected post-closure time divisions.

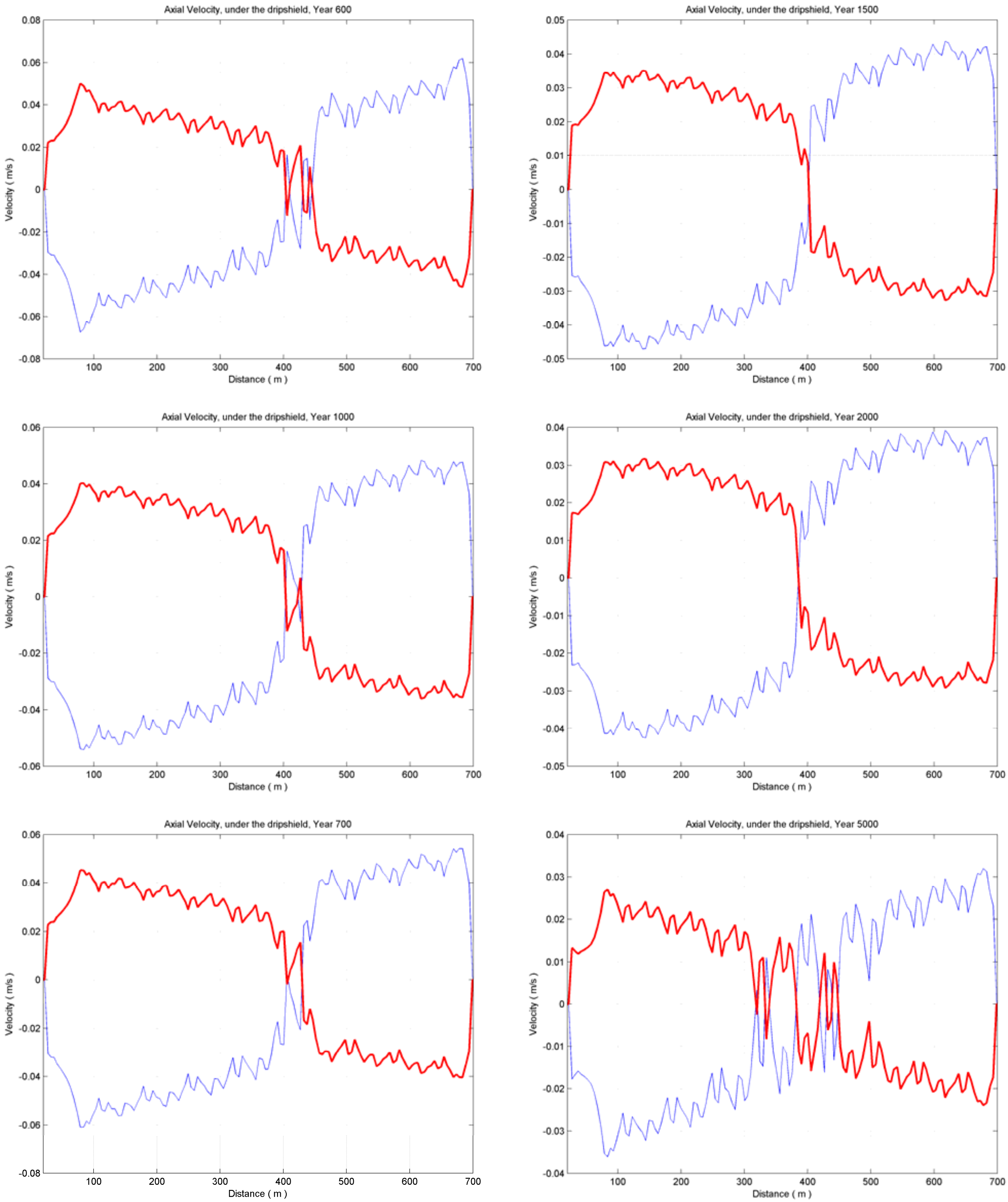

Figure 2-13. Axial air velocity variation under the drip shield at selected post-closure time divisions.

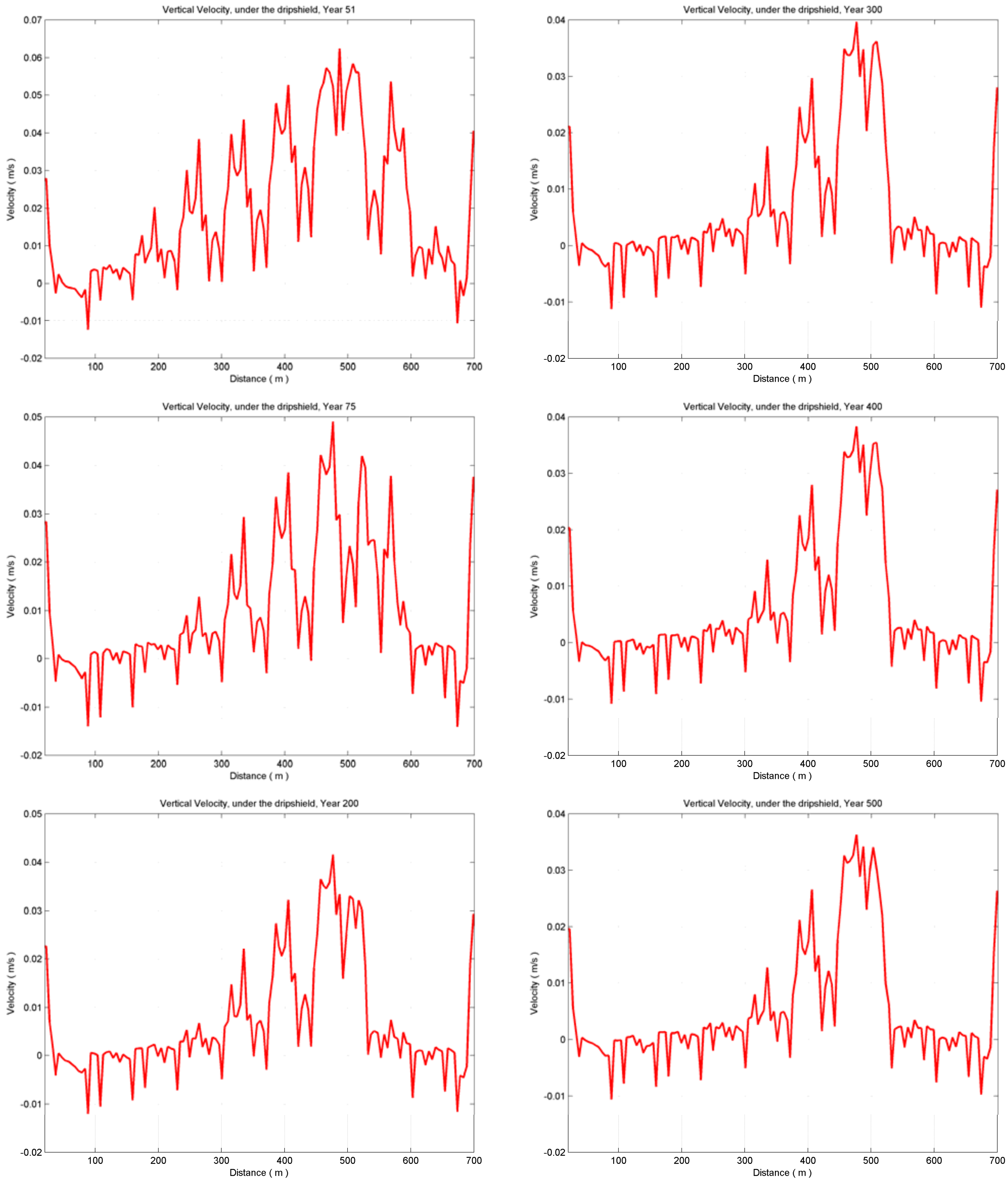

Figure 2-14. Transversal air velocity variation above the drip shield at selected post-closure time divisions.

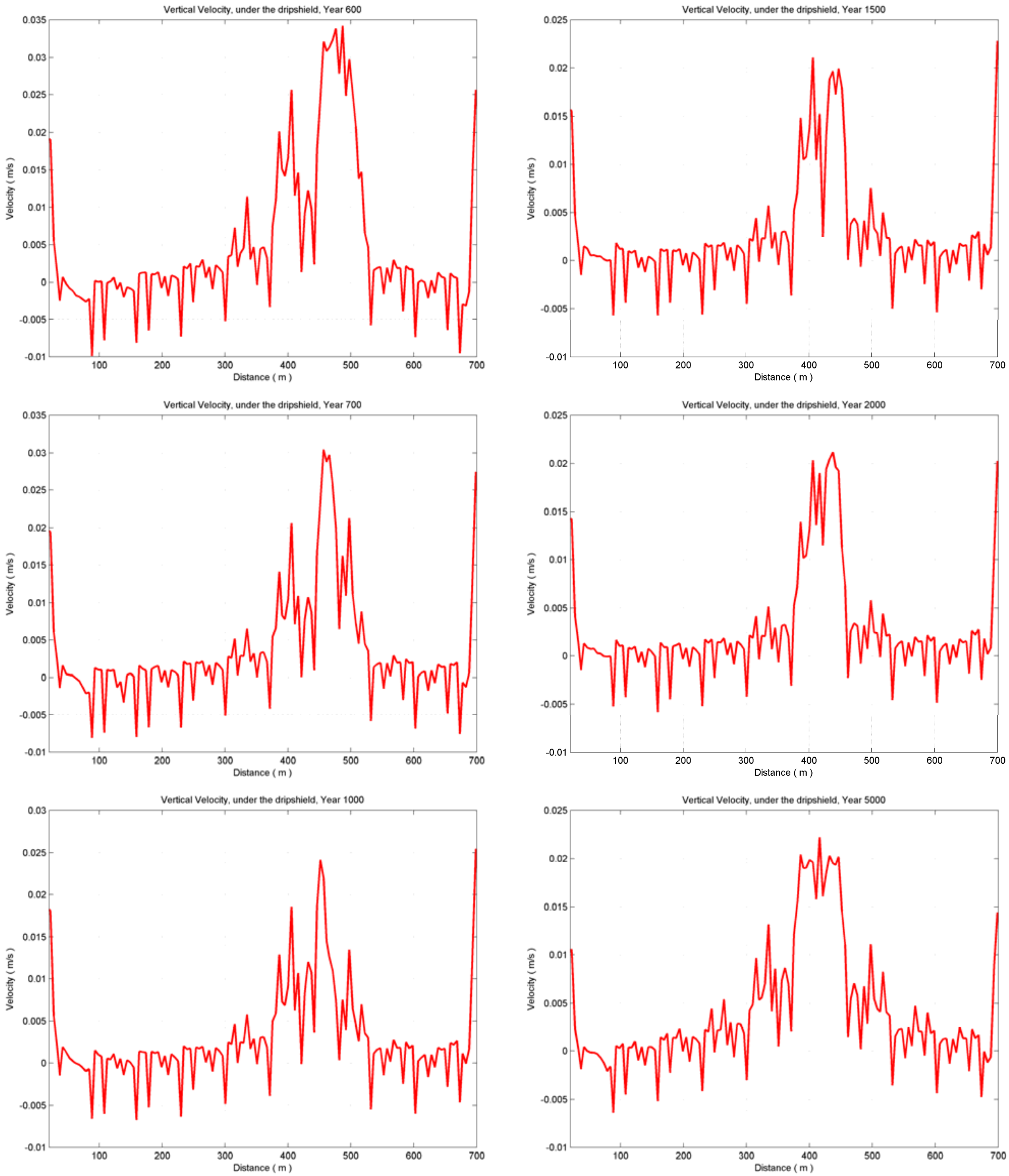

Figure 2-15. Transversal air velocity variation above the drip shield at selected post-closure time divisions.

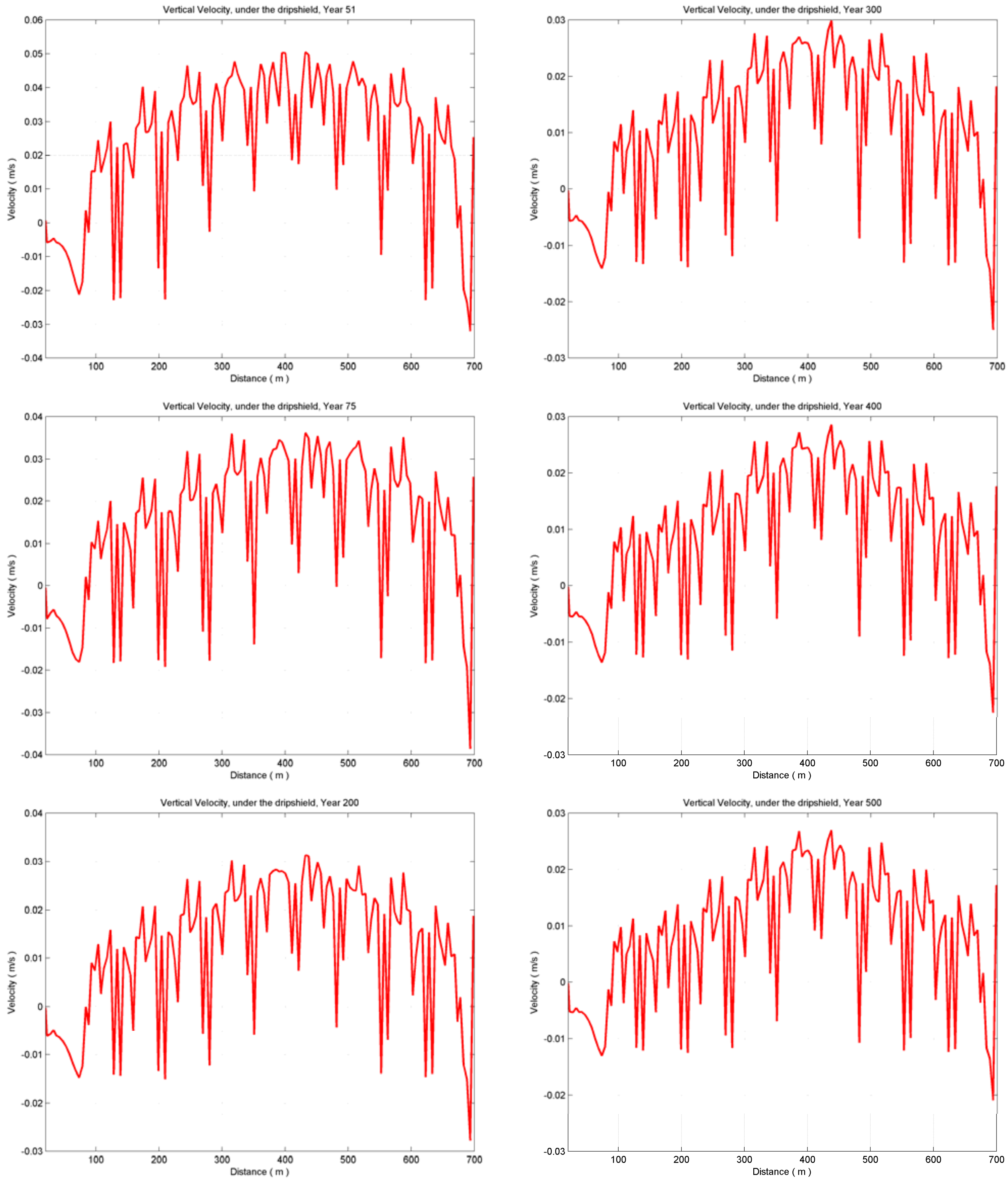

Figure 2-16. Transversal air velocity variation under the drip shield at selected post-closure time divisions.

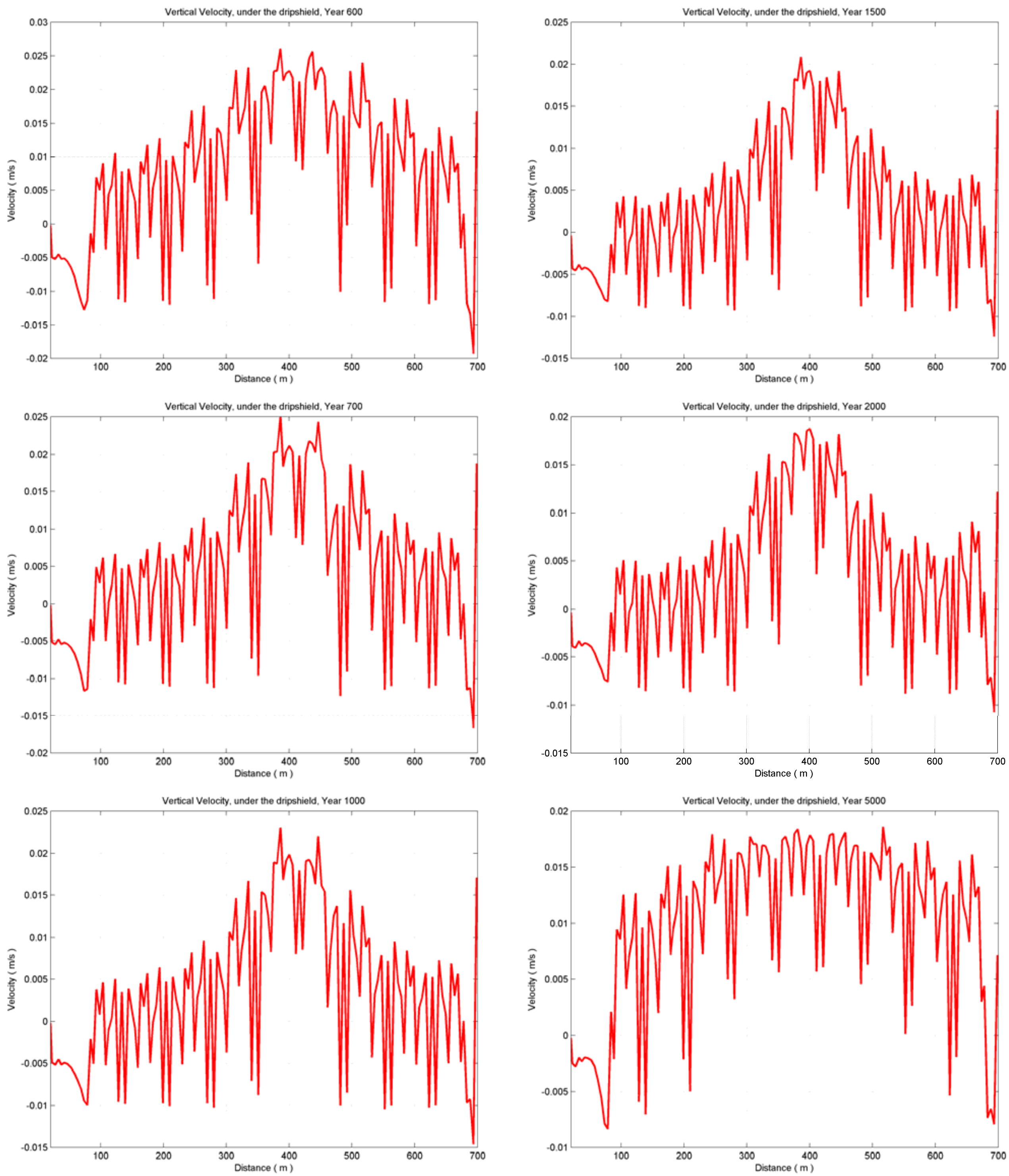

Figure 2-17. Transversal air velocity variation under the drip shield at selected post-closure time divisions.

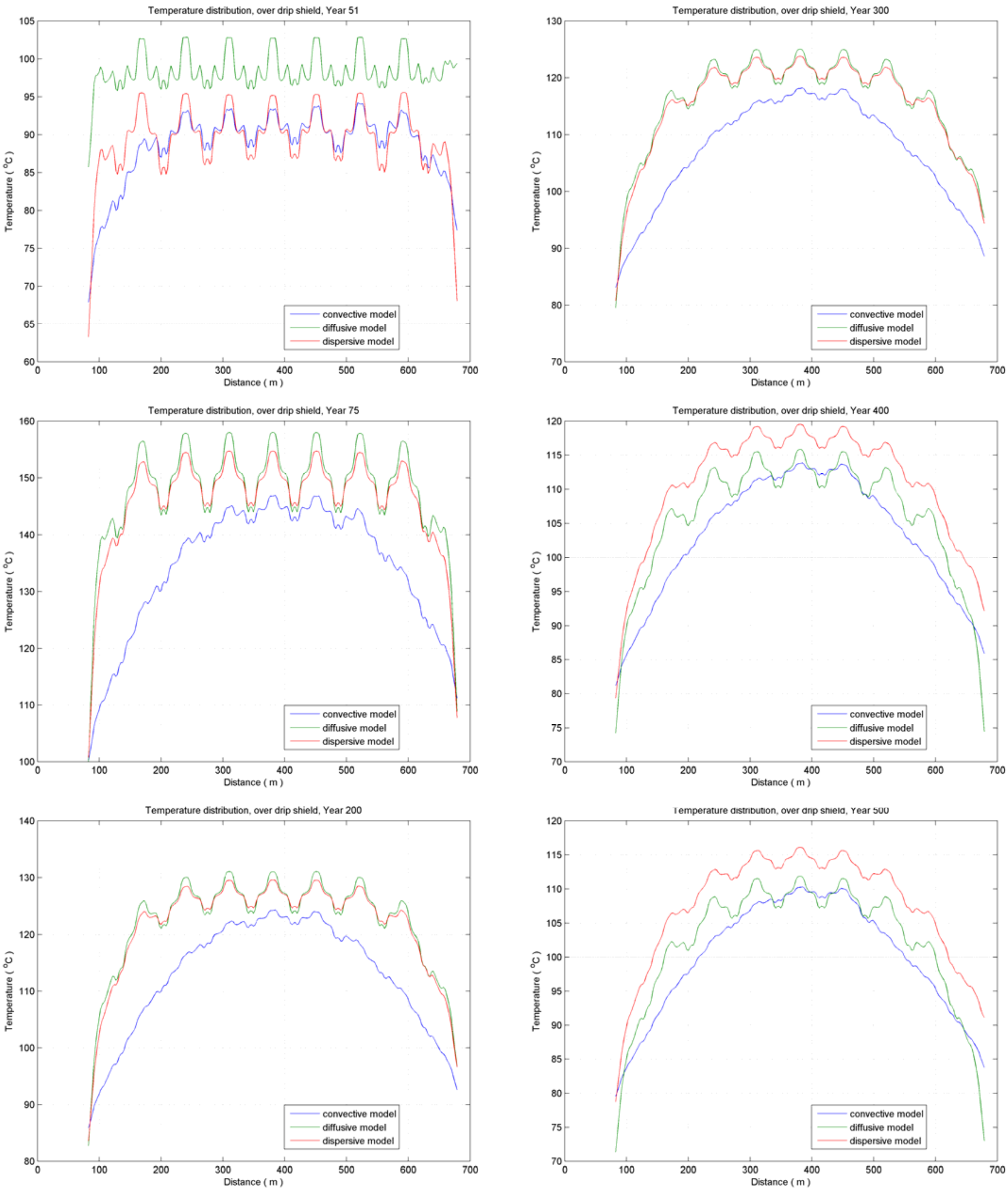

Figure 2-18. Drift wall temperature distribution in the airspace above the drip shield at selected post-closure time divisions.

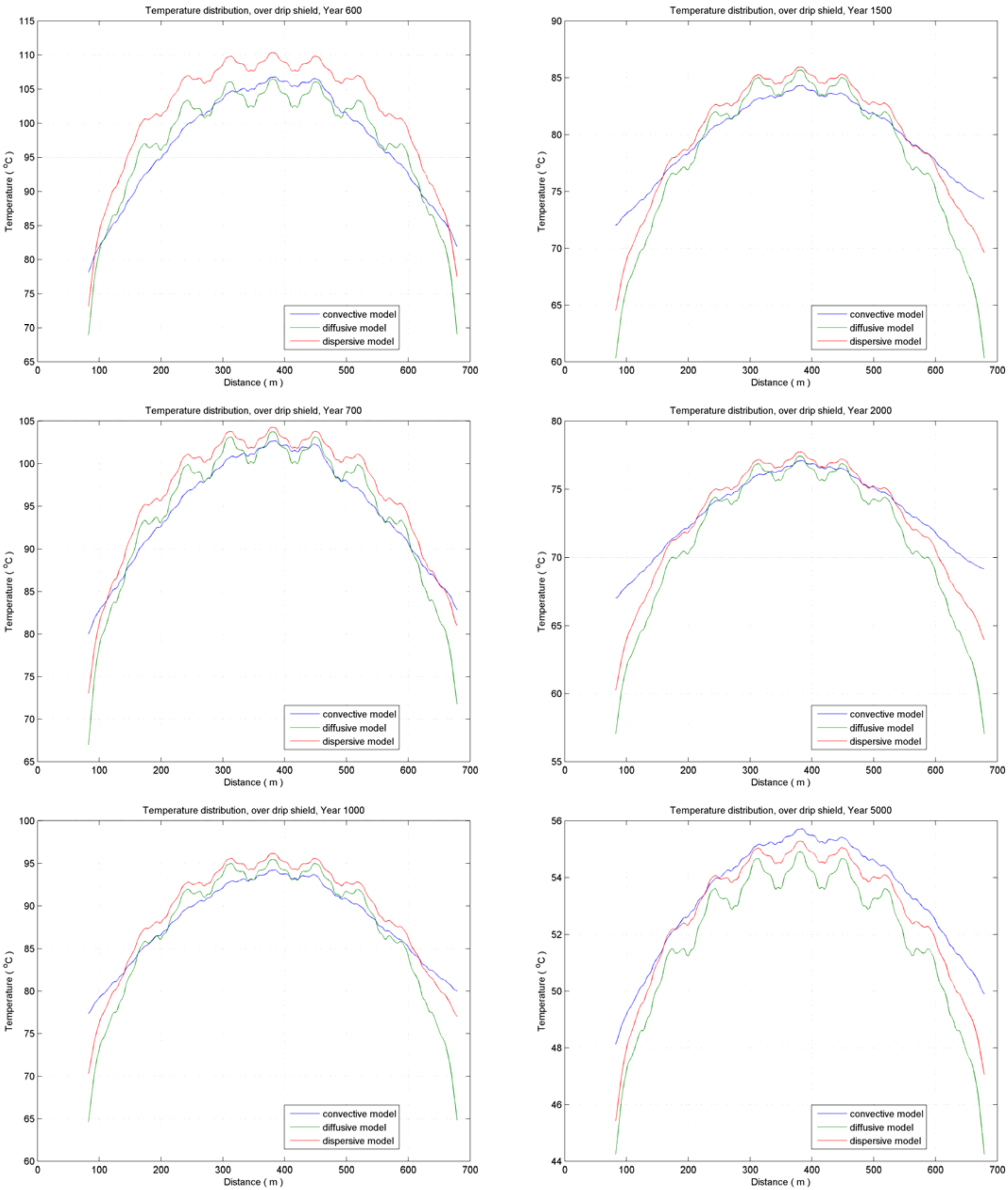

Figure 2-19. Drift wall temperature distribution in the airspace above the drip shield at selected post-closure time divisions.

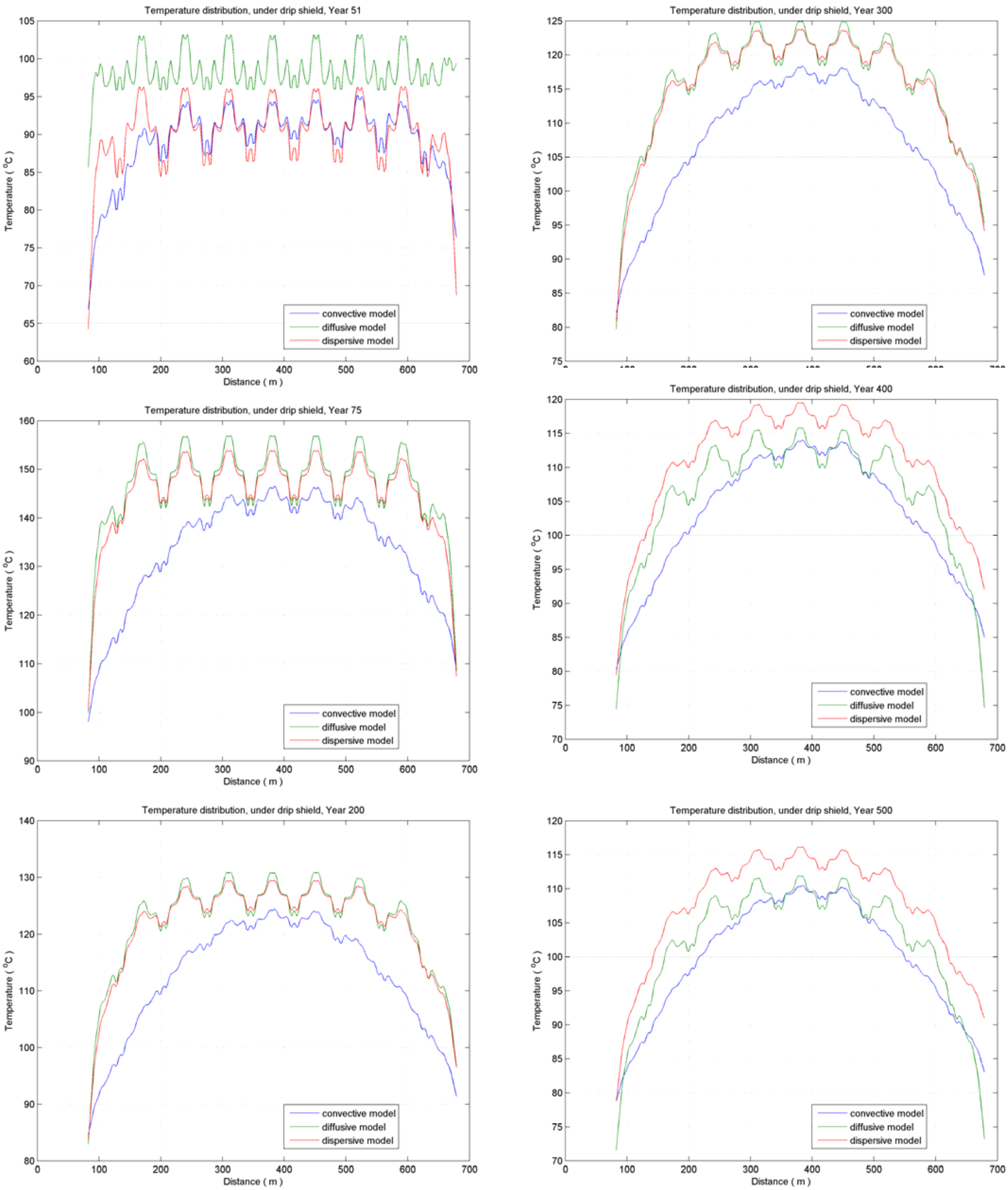

Figure 2-20. Drift invert temperature distribution in the airspace under the drip shield at selected post-closure time divisions.

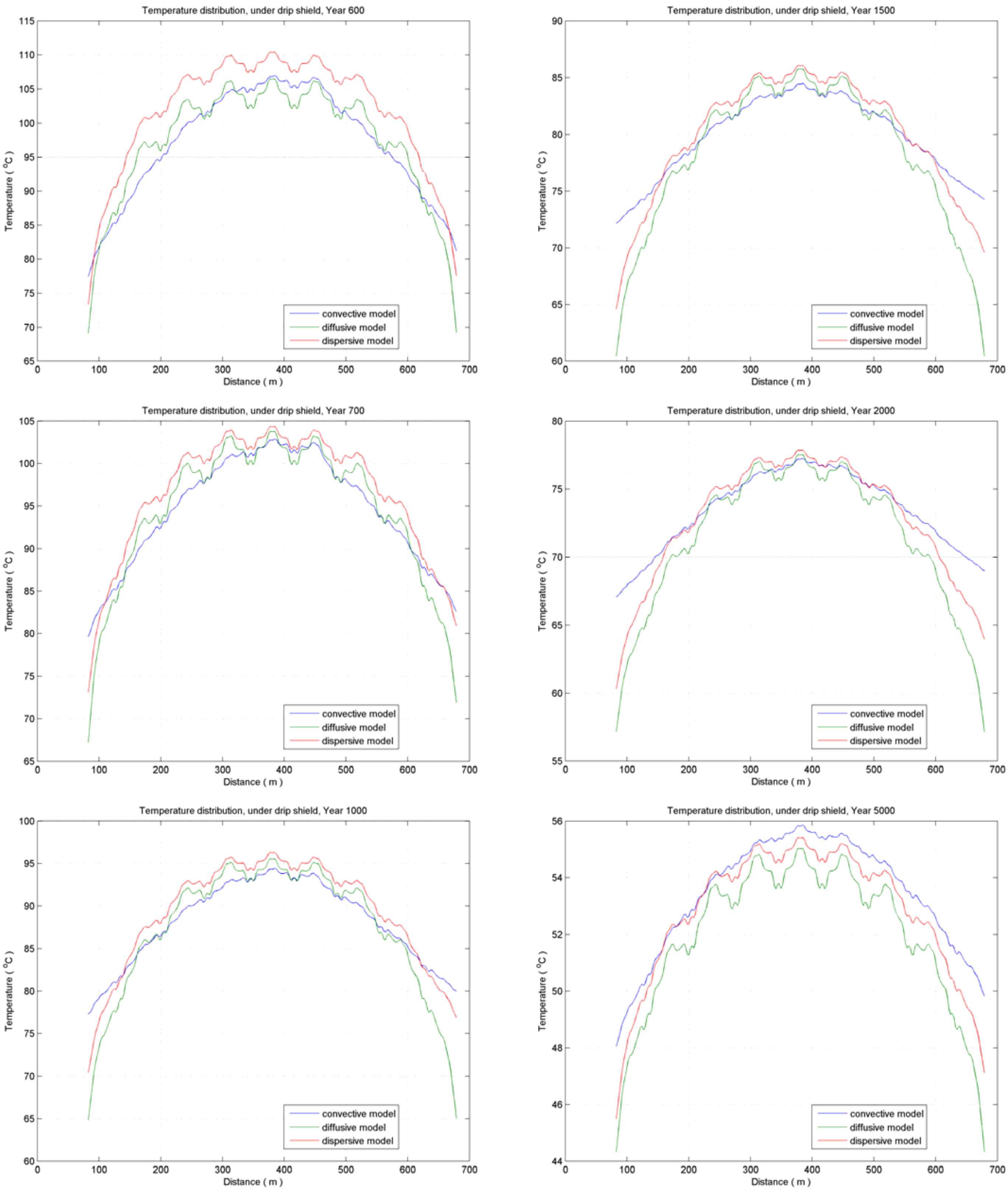

Figure 2-21. Drift invert temperature distribution in the airspace under the drip shield at selected post-closure time divisions.

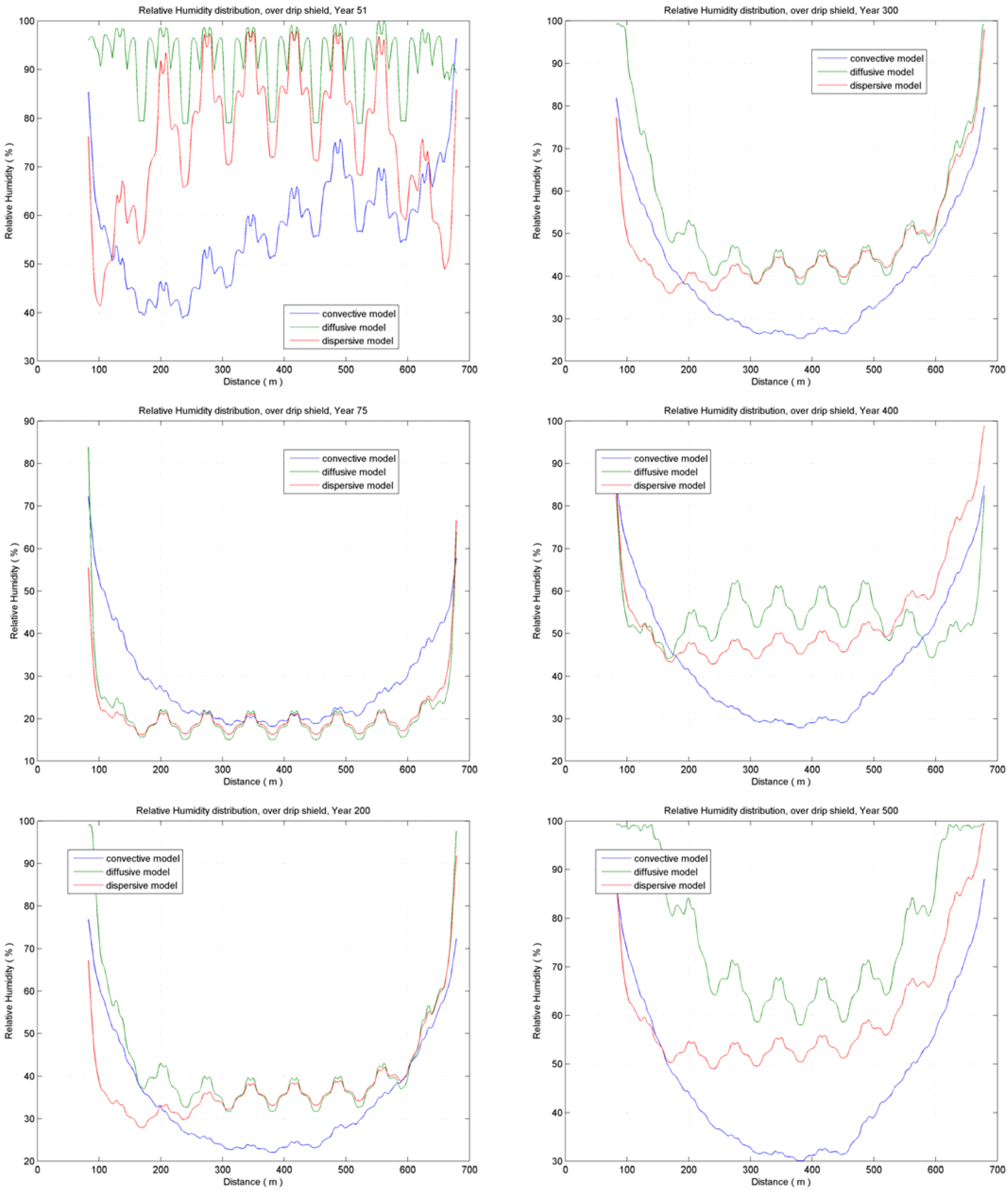

Figure 2-22. Drift wall relative humidity distribution in the airspace above the drip shield at selected post-closure time divisions.

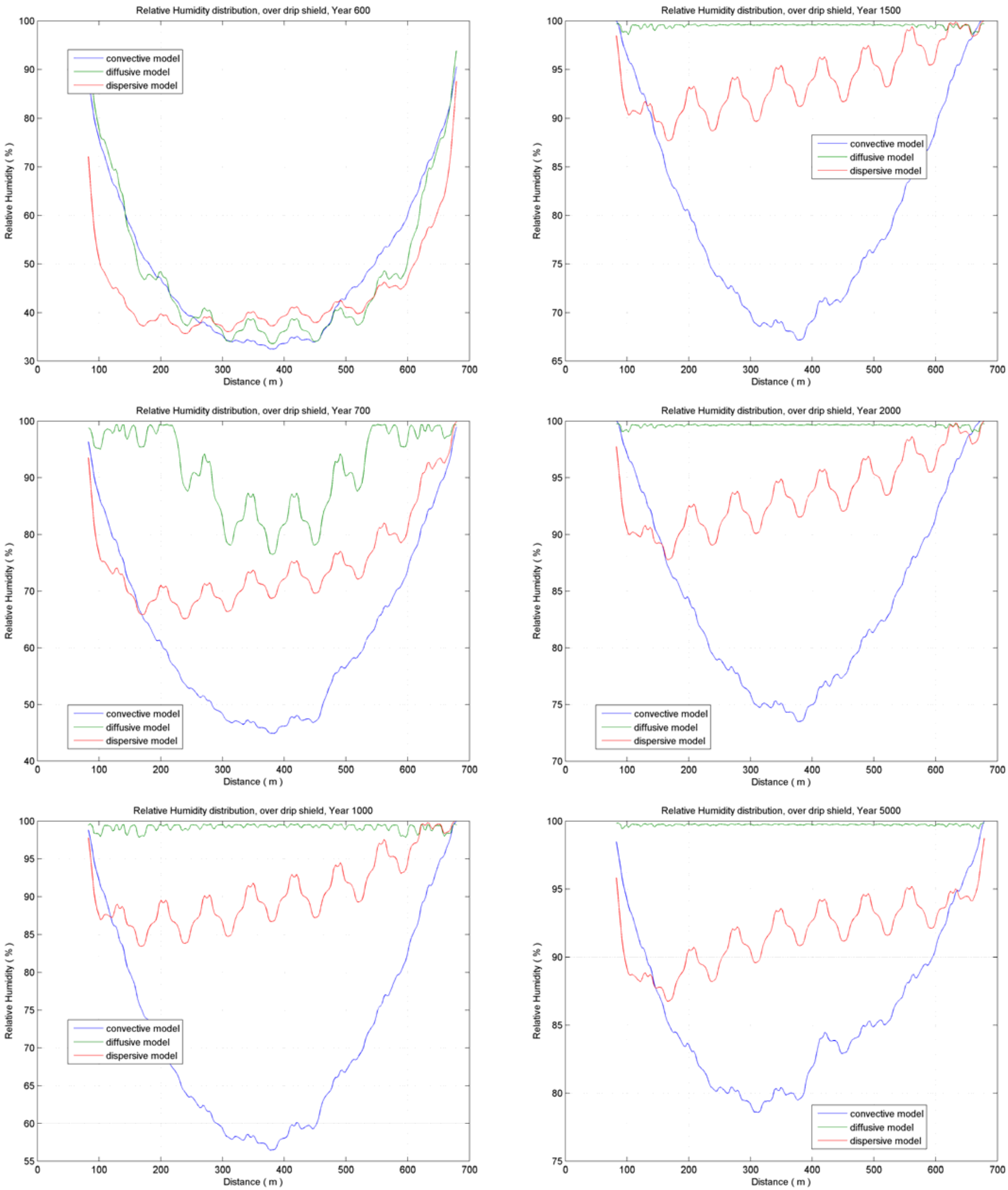

Figure 2-23. Drift wall relative humidity distribution in the airspace above the drip shield at selected post-closure time divisions.

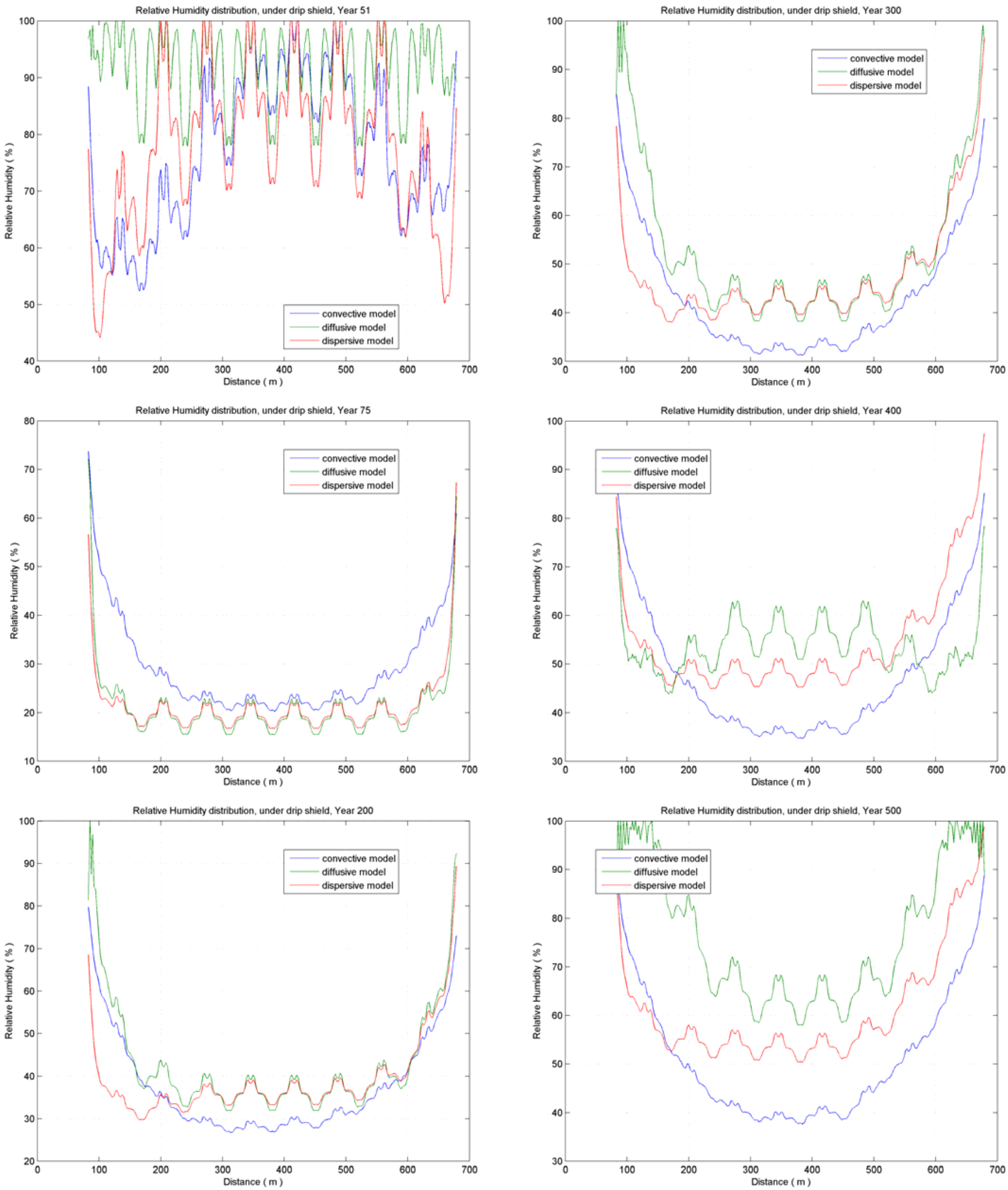

Figure 2-24. Drift invert relative humidity distribution in the airspace under the drip shield at selected post-closure time divisions.

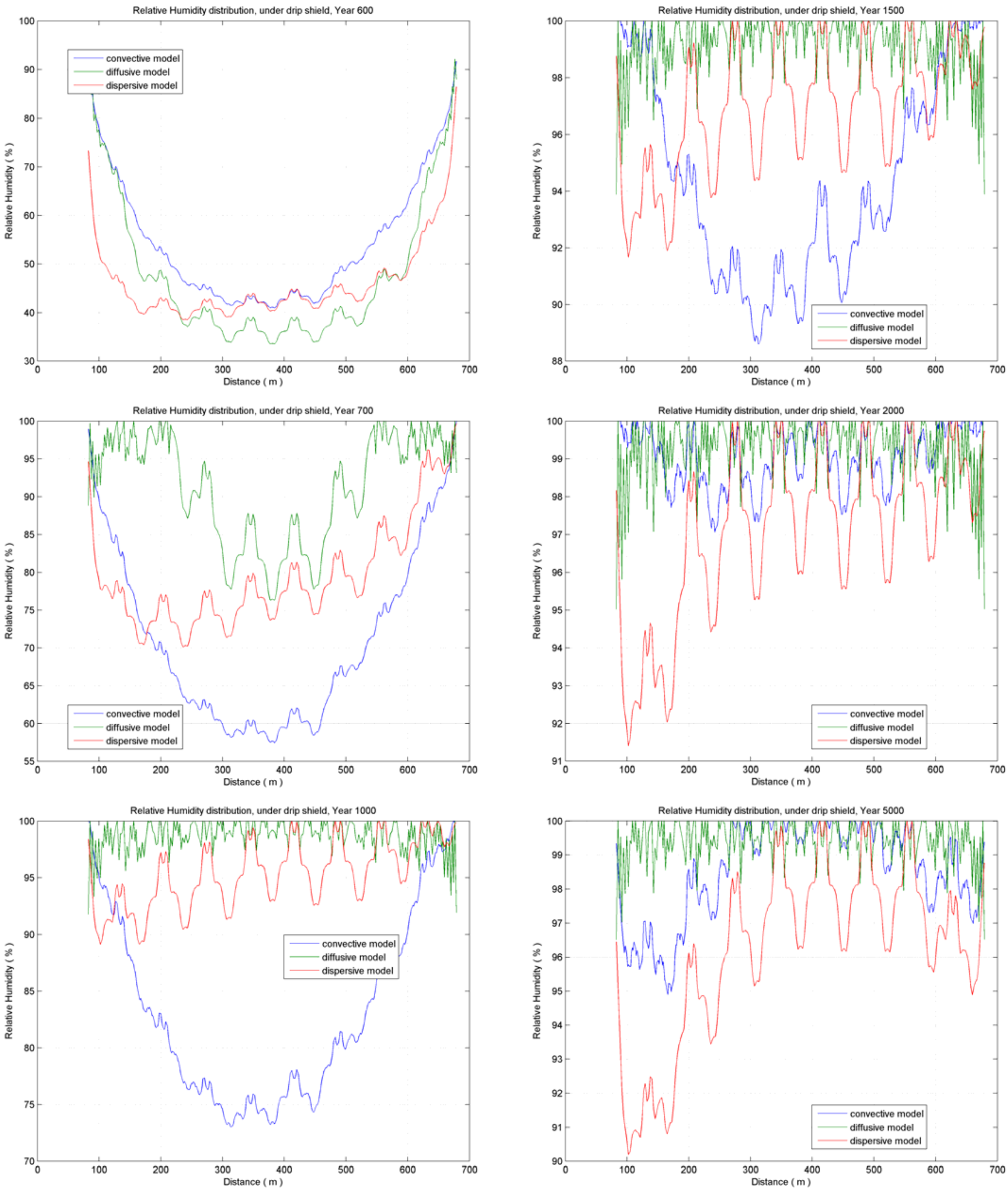

Figure 2-25. Drift invert relative humidity distribution in the airspace under the drip shield at selected post-closure time divisions.

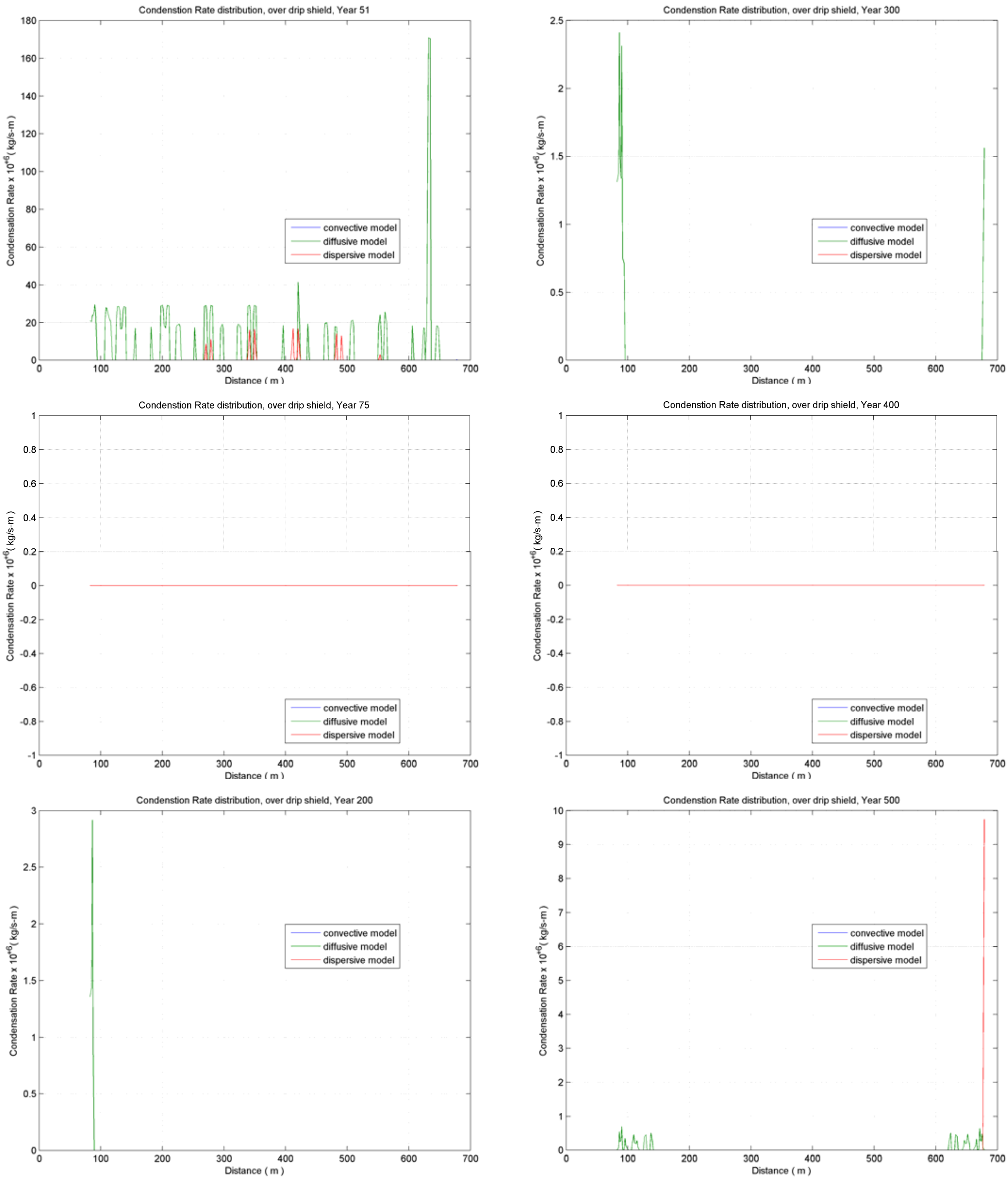

Figure 2-26. Condensation rate distribution above the drip shield at selected post-closure time divisions.

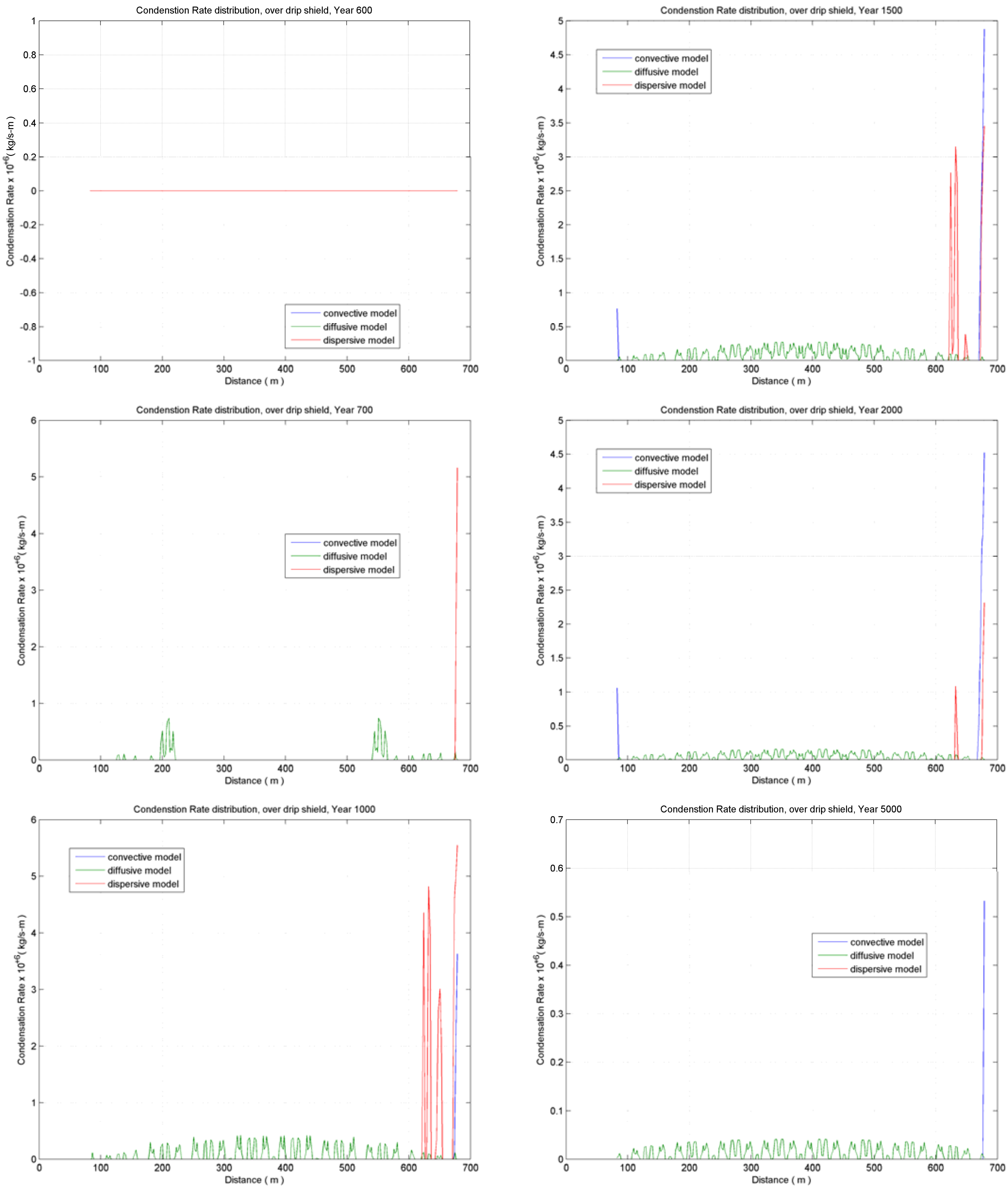

Figure 2-27. Condensation rate distribution above the drip shield at selected post-closure time divisions.

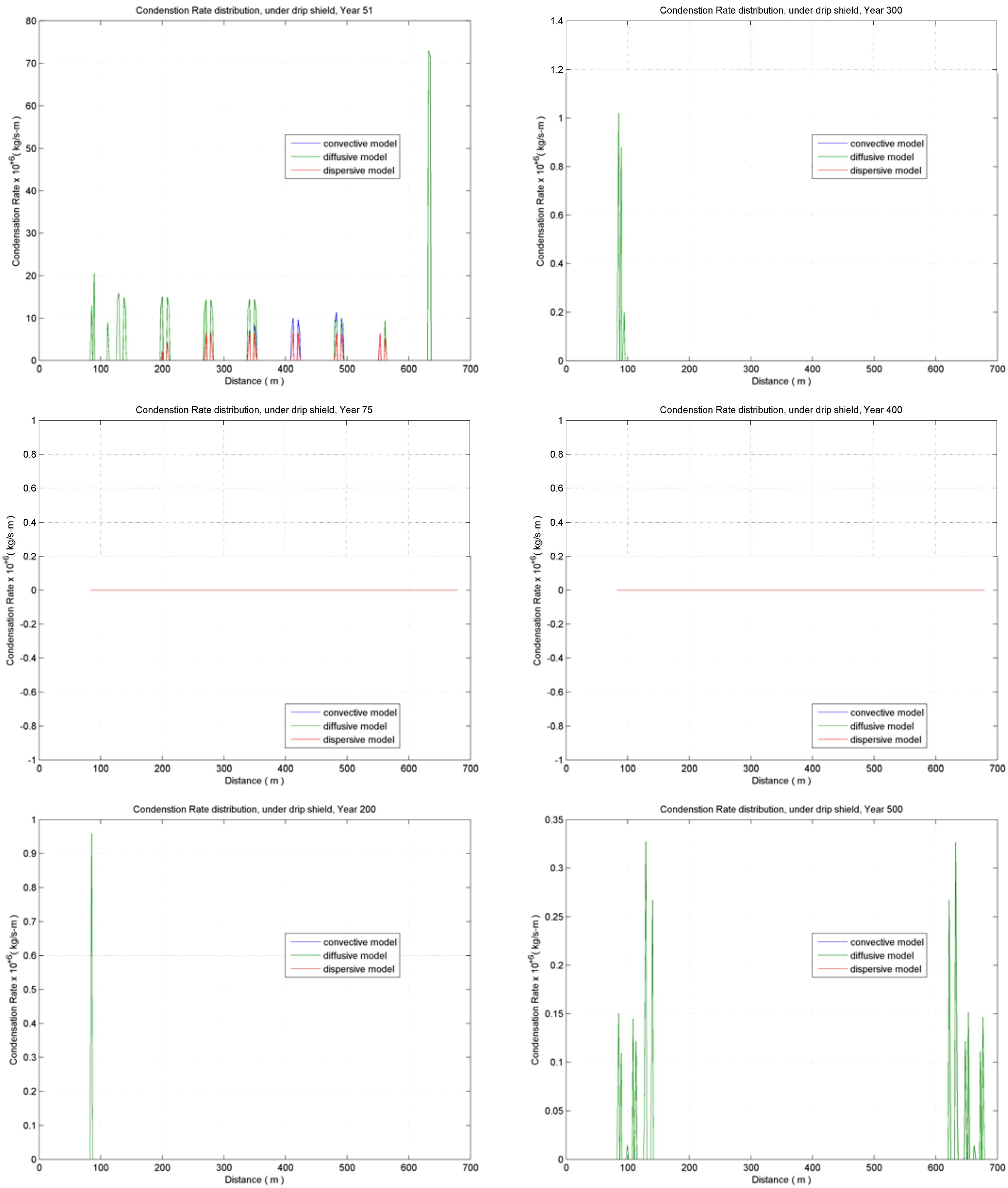

Figure 2-28. Condensation rate distribution under the drip shield at selected post-closure time divisions.

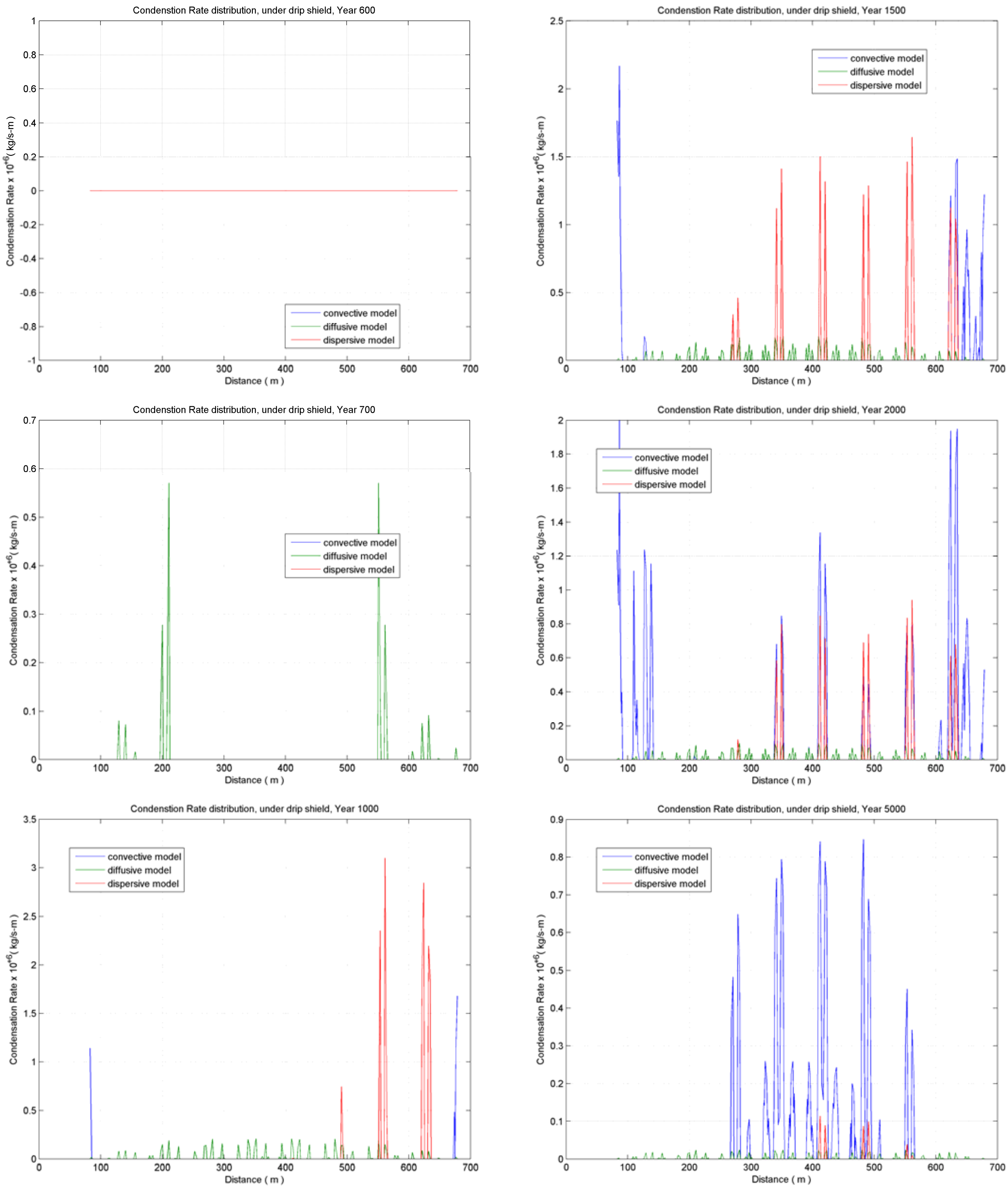

Figure 2-29. Condensation rate distribution under the drip shield at selected post-closure time divisions.

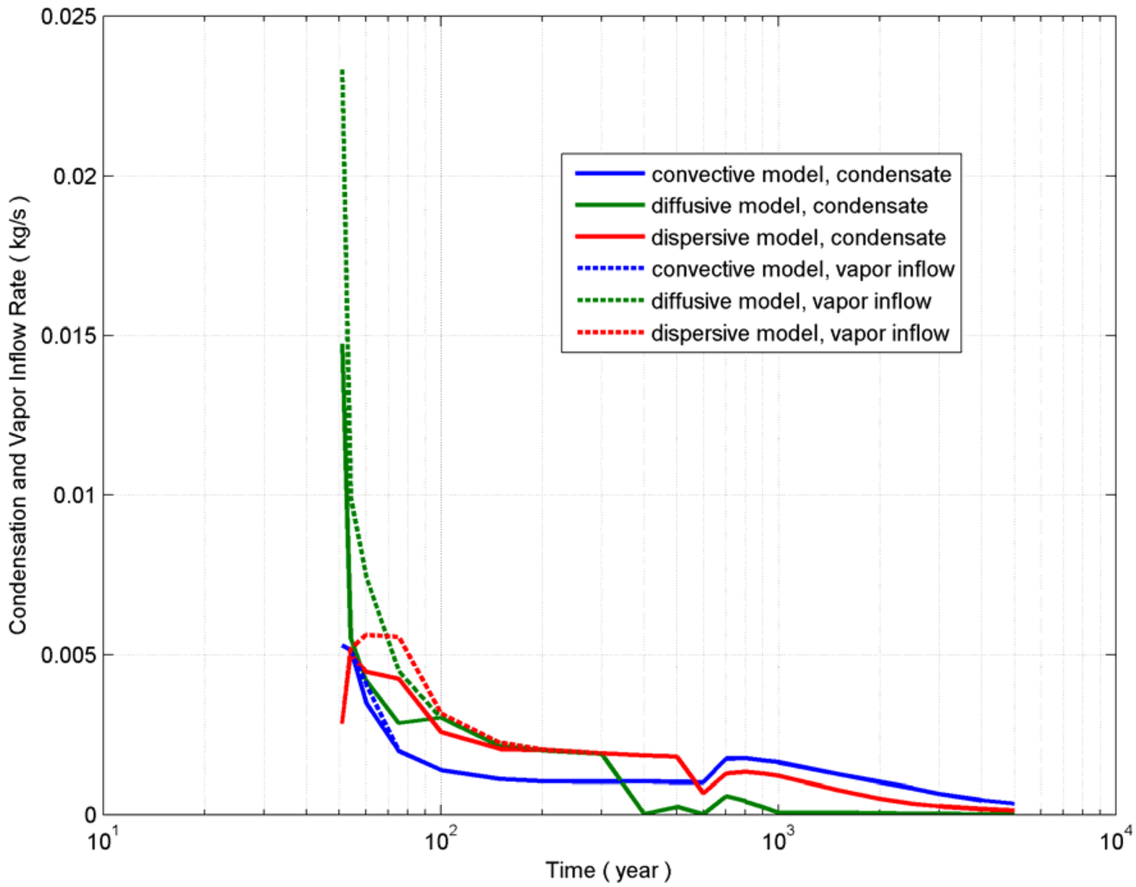

Figure 2-30. The evolution of total condensation rate (solid line) and vapor inflow rate (dashed line) in the emplacement drift.

2.3. Comments on DOE response to related contentions

Reviewed the DOE's response to all contentions and provided technical comments on the ones that articulate what Nye County has been arguing over the years. The comments were given in the January 2009 Progress Report.

Reviewed the DOE's answers to Nye County safety contentions 1 and 2 and provided comments. The comments were given in the February 2009 Progress Report.

3. <u>Task 3 – Corrosion-related studies</u>

Corrosion is strongly related to the temperature, relative humidity, and the presence of liquid water, its mobility and chemical composition. Our task was to define temperature, relative humidity, and the rate of condensation as functions of time and location in the selected emplacement drift. We linked this task to the thermal-hydrologic model studies, as the waste package storage environment is a function of site input as well as design parameters. Figure 3-1 illustrates this relationship.

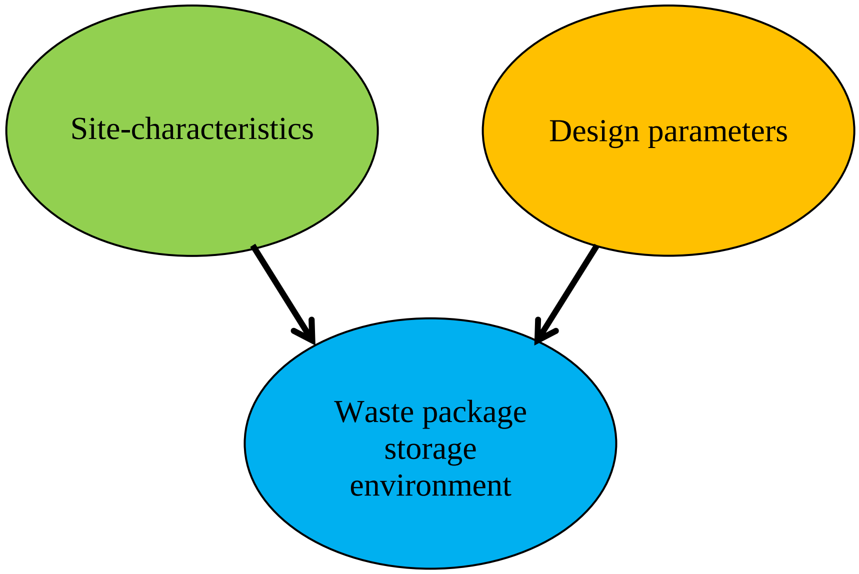

Figure 3-1. Relationship between waste package storage environment and model parameters.

The most realistic and scientifically justified model is the convective one, which uses the least amount of simplifying assumptions. We use the results of this model as our best prediction. Taking the final, fully iterated results of this convective model configuration (model arrangement 18 in Table 1), three waste package locations were identified as the most critical, two are at hot and humid locations (in Tables 3-1 and 3-2) and one is in a wet and humid location (in Table 3-3). The input data for corrosion study are summarized for three waste package locations in Table 3-1 through Table 3-3. Each table includes time, waste package surface temperature and relative humidity values, and rate of condensation formation at the waste package location. The condensation occurs on the drift side wall surfaces and on the surface of the invert. The 15-m unheated section at the exit side is not long enough to drain all the moisture inflow from the rockmass into the drift airspace and to prevent wet condition at waste package locations. This is in disagreement with the LA abstraction models assertion that none of the waste packages experience a wet environment prior to year 2000. These results show that waste packages at the exit side could be in a wet environment as early as year 800. However, the condensation formation is not on the drip shield nor on the waste package itself, but on the invert. Water may not come in contact with the waste packages since condensation may drain out. The condensation on the drift wall outside the drip shield may reach the invert or simply imbibe into the rockmass. However, the pallet can be in wet condition and the waste package surface will be in a high-humidity air with higher than 90% relative humidity from early time periods. Further studies on corrosion by Nye County subject matter expert is recommended.

We consider the presence of condensate water under the drip shield a major finding. Although it may not cause aqueous corrosion, but the drainage water may transport escaped radionuclides. Any early failure under the entire drift length may deliver contaminated gas that can come in contact with water and transported by drainage into the water table. This mechanism is completely left out from the LA transport models.

Table 3-1. Hot and humid environmental condition at 44BWR waste package surface. Condensation rate is the total at the waste package location, 372.8 m from entrance.

Time	Temperature	Vapor Pressure	Relative Humidity	Condensation Rate	WP heat
(year)	(^{o}C)	(kPa)	(%)	(kg/s x 10^{-6})	(W)
51	107.110	69.176	53.260	0.000	1432.20
54	133.910	88.401	29.151	0.000	1373.50
60	149.820	88.403	18.662	0.000	1270.70
75	153.850	88.376	16.764	0.000	1062.60
100	146.730	79.542	18.256	0.000	832.41
150	134.710	67.405	21.712	0.000	599.83
200	127.900	62.160	24.514	0.000	492.10
300	121.180	59.600	28.918	0.000	389.28
400	116.420	57.574	32.518	0.000	328.07
500	112.610	55.611	35.576	0.000	286.45
600	108.880	53.706	38.925	0.000	252.17
700	104.670	65.098	54.502	0.000	225.49
800	101.330	65.005	61.185	0.000	202.72
900	98.436	63.090	65.858	0.000	183.62
1,000	95.743	61.185	70.436	0.000	167.46
1,500	85.359	51.079	87.134	0.000	115.80
2,000	78.038	41.733	95.455	0.191	91.08
2,500	72.381	33.174	96.116	2.323	78.59
3,000	67.763	27.221	96.301	2.217	71.73
4,000	61.168	20.266	96.405	1.603	64.15
5,000	56.391	16.226	96.469	1.226	59.25

Table 3-2. Hot and humid environmental condition at DHLW waste package surface. Condensation rate is the total at the waste package location, 388.6 m from entrance.

Time	Temperature	Vapor Pressure	Relative Humidity	Condensation Rate	WP heat
(year)	(^oC)	(kPa)	(%)	(kg/s x 10^{-6})	(W)
51	97.765	68.875	73.661	44.276	199.71
54	125.450	88.401	37.567	0.000	191.51
60	142.280	88.403	22.942	0.000	177.18
75	147.570	88.401	19.831	0.000	148.16
100	141.540	80.126	21.231	0.000	116.07
150	130.630	67.916	24.670	0.000	83.64
200	124.400	62.653	27.495	0.000	68.62
300	118.310	60.059	31.924	0.000	54.28
400	113.930	58.011	35.534	0.000	45.75
500	110.370	56.049	38.641	0.000	39.94
600	106.850	54.118	42.032	0.000	35.16
700	102.760	65.591	58.703	0.000	31.44
800	99.595	65.365	65.451	0.000	28.27
900	96.831	63.397	70.140	0.000	25.60
1,000	94.231	61.419	74.755	0.000	23.35
1,500	84.150	51.085	91.382	0.000	16.15
2,000	77.208	41.491	98.198	6.100	12.70
2,500	71.618	32.967	98.679	7.393	10.96
3,000	67.039	27.044	98.768	6.587	10.00
4,000	60.480	20.119	98.783	5.057	8.94
5,000	55.727	16.100	98.785	4.080	8.26

Table 3-3. Wet and humid environmental condition at 44BWR waste package surface. Condensation is the total at the waste package location, 655.5 m from entrance (last WP at exit location).

Time	Temperature	Vapor Pressure	Relative Humidity	Condensation	WP heat
(year)	(^{o}C)	(kPa)	(%)	(kg/s x 10^{-6})	(W)
51	93.219	38.940	49.208	1.007	1432.20
54	112.010	80.580	52.587	0.000	1373.50
60	119.720	88.402	44.920	0.000	1270.70
75	121.060	84.154	40.990	0.000	1062.60
100	114.060	69.909	42.638	0.000	832.41
150	103.610	58.780	51.065	0.000	599.83
200	97.752	54.030	57.811	0.000	492.10
300	92.813	51.245	65.748	0.000	389.28
400	89.513	49.432	71.826	0.000	328.07
500	86.994	47.631	76.243	0.000	286.45
600	84.752	45.737	79.901	0.000	252.17
700	85.529	52.731	89.354	0.000	225.49
800	84.653	52.019	91.229	9.199	202.72
900	83.344	49.962	92.266	16.713	183.62
1,000	81.958	47.709	93.103	21.975	167.46
1,500	75.674	37.650	94.956	26.627	115.80
2,000	70.183	29.970	95.418	22.258	91.08
2,500	65.248	24.106	95.325	17.042	78.59
3,000	61.111	20.011	95.435	11.808	71.73
4,000	55.115	15.112	95.477	4.504	64.15
5,000	50.702	12.182	95.387	1.376	59.25

4. Reports, Publications, and presentations

We submitted 12 monthly progress reports for FY 2009.

Nye County's contractor meeting

Prepared presentation material for the Nye County's contractor meeting on May 4th and 5th. Attended the Nye County's contractor meeting on May 4th and 5th and presented our current activities, findings and future tasks. The presentation slides are given in Attachment 1(May 2009).

Journal of Nuclear Technology

Completed resolving the review comments provided by the JNT editor for the paper entitled "Temperature, Humidity and Air Flow in The Emplacement Drifts Using Convection and Dispersion Transport Models". The revised manuscript was accepted for publication by JNT, and the paper is waiting for proofing.

Online Journal of Heat and Mass Transfer

Continued working on resolving the review comments provided by the HMT editor for the paper entitled "Coupled In-Rock and Approximate In-Drift Models Using a Surrogate Dispersion Process" submitted to online Journal of Heat and Mass Transfer and started working on resolving the comments and revising the paper. The work is in progress.

Public comment to NWTRB and Mark Holt

Submitted public comment to the Nuclear Waste Technical Review Board and also to Mark Holt at Congressional Research Service with Nye County's permission. The public comment outlines the idea of using the Yucca Mountain site as a staged repository starting as a ventilated storage facility. Suggestion was also made to the Organizing Committee of the next International High-Level Radioactive Waste Management Conference in 2011 regarding a session on the topic of a staged storage at Yucca Mountain as outlined in the public comment (see Attachment 1, June 2009 Progress Report).

Submitted a conference paper and prepared a poster of the THOUGH 2009 paper

Completed and submitted the paper entitled "Development and Applications of a Turbulent Transport Network Model Coupled with TOUGH2" which was presented at the TOUGH 2009 symposium on September 14, 2009, Berkeley, California. The paper was a short, but revised version of a publication at the High-Level Radioactive Waste Management Conference in 2008 focusing on model arrangement 19 in Table 1. Prepared the poster presentation material for this event. The components of this poster presentation were submitted to Nye County in the September 2009 Progress Report.

NWTRB meeting on September 23, 2009

Attended the NTWRB meeting September 23, 2009 on closing the nuclear fuel cycle. A brief trip report was provided in the September 2009 Progress Report.

References

1. Sandia National Laboratory (SNL), (2008). “Multiscale Thermohydrologic Model.” ANL-EBS-MD-000049, Rev. 03, Las Vegas, Nevada: Sandia National Laboratories., 2008.
2. Danko, G., and Bahrami, D., “The Impact of Thermal Seepage on the Hydraulic System of Yucca Mountain,” Devil’s Hole Workshop, Death Valley, California, 2005.
3. Sandia National Laboratory (SNL), (2007). “In-drift natural convection and condensation.” Yucca Mountain Project Report, MDL-EBS-MD-000001 REV 00 AD 01, Las Vegas, Nevada: Sandia National Laboratories., 2007.
4. Webb, S. W. and Itamura M. T., (2004). “Calculation of Post-Closure Natural Convection Heat and Mass Transfer in Yucca Mountain Drifts.” Proceedings of ASME, Heat Transfer/Fluid Engineering, July 11-15, Charlotte, NC.
5. Birkholzer, J.T., Halecky, N., Webb, S.W., Peterson, P.F., Bodvarsson, G.S., (2008) "A Modeling Study Evaluating the Thermal-Hydrological Conditions in and Near Waste Emplacement Tunnels at Yucca Mountain." Journal of Nuclear Technology, July, 163, 2008.
6. Danko, G., Bahrami, D., and Birkholzer, J. T., (2006). “The Effect of Unheated Sections on Moisture Transport in the Emplacement Drift,” Proceedings, Int. High-Level Radioactive Waste Management Conference, April 30-May 4, Las Vegas, NV, pp.1-8.
7. Danko, G., and Bahrami, D., (2006). “The Effect of Pre-Closure Ventilation on the Environmental Conditions at Yucca Mountain,” Proceedings, Int. High-Level Radioactive Waste Management Conference, April 30-May 4, Las Vegas, NV, pp.1-8.
8. Danko, G., and Bahrami, D., (2006). “Barometric Pressure Variation Effects on Emplacement Drift Environmental Conditions at Yucca Mountain,” Proceedings, Int. High-Level Radioactive Waste Management Conference, April 30-May 4, Las Vegas, NV, pp.1-8.
9. Danko G., Bahrami D., Birkholzer J., (2008). "Comparison of Axial Convection and Equivalent Dispersion Models in Emplacement Drifts." Proceedings of the 12th International High-Level Nuclear Waste Conference, IHLRWM, 2008, Las Vegas, NV, September 7-11, 2008, pp. 299-307.
10. Danko G., Bahrami D., (2008). "Large-Eddy, Post-Closure Natural Convection CFD Model for Yucca Mountain." Proceedings of the 12th International High-Level Nuclear Waste Conference, IHLRWM, 2008, Las Vegas, NV, September 7-11, 2008, pp. 339-347.
11. Danko, G., Birkholzer J., Bahrami, D., Halecky, N. (accepted and edited for publication in 2009). "Temperature, Humidity and Air Flow in The Emplacement Drifts Using Convection and Dispersion Transport Models." Journal of Nuclear Technology.
12. July 2009 Progress Report to Nye County
13. Danko, G., Birkholzer, J. T., Bahrami, D. (2009). "Development and Applications of a Turbulent Transport Network Model Coupled with TOUGH2." TOUGH 2009 Symposium, September 14, 2009, Berkeley CA, pp. 1-8.
14. LSN: DEN001584610 SNL 2008. Performance Confirmation Plan. TDRPCS-SE-000001 REV 05 AD01 ACN01. Las Vegas, Nevada: Sandia National Laboratories. ACC: DOC.20080227.003
15. LSN: DEN001592183 OCRWM 2008. Yucca Mountain Repository License Application, General Information and Safety Analysis Report. DOE/RW-0573 REV 0. June 2008. U.S. Department of Energy, Office of Civilian Radioactive Waste Management, MOL.20080501.0021.
16. Annual Letter Report for FY2008 to Nye County

17. Danko, G., Birkholzer, J., and Bahrami, D. (2008). "Coupled In-Rock and In-Drift Hydrothermal Model Study for Yucca Mountain." Journal of Nuclear Technology, July, Vol. 163, pp. 110-128.
18. Danko, G., Walton, J., and Bahrami, D. (2008). "Increased Storage Capacity At Yucca Mountain Favors Thermal Management For A Cold Repository." Journal of Nuclear Technology, July, Vol. 163, pp. 47-61.
19. Danko, G., 2008, MULTIFLUX V5.0 Software Quantification Documents. Software Tracking Number: 1002-5.0-00, Prepared for the Berkeley National Laboratory at University of Nevada, Reno.
20. Welty, J. R., Wicks, C.E., and Wilson, R.E. (1984). "Fundamentals of Momentum, Heat, and Mass Transfer." 3rd edition, Wiley and Sons, pp. 612-614, 360.
21. Birkholzer, J., N. Halecky, S.W. Webb, P.F. Peterson, G.S. Bodvarsson, (2006). "The Impact of Natural Convection on Near-Field TH Processes at Yucca Mountain." Proceedings, 11th International High-Level Nuclear Waste Conference, April, Las Vegas, NV.
22. March 2009 Progress Report to Nye County.